

Correlation between multiple scattering angle and ionization energy loss for relativistic electrons

M.V. Bondarenko*

*NSC Kharkov Institute of Physics and Technology, 1 Academic St., 61108 Kharkov, Ukraine and
V.N. Karazine Kharkov National University, 4 Svobody Sq., 61077 Kharkov, Ukraine*

(Dated: November 20, 2020)

A correlation between the angle of multiple scattering and the ionization energy loss for relativistic electrons in an amorphous medium is evaluated based on a solution of the transport equation. The correlation is found to be the strongest in the large deflection angle region, but also sizable at typical deflection angles, where it leads to a broadening of the angular distribution with the increase of the energy loss. The mean energy loss as a function of the deflection angle grows quadratically with the increase of the latter, but the proportionality coefficient changes when passing from the small- to the large-deflection angle region.

PACS numbers: 34.50.Bw, 11.80.La

I. INTRODUCTION

Fast charged particles passing through amorphous matter deflect and lose energy by elastic and inelastic collisions with individual atoms. The corresponding deflection angle distribution was calculated by Molière [1], and the ionization energy loss distribution, by Landau [2], with subsequent refinements summarized in [3–10]. Strictly speaking, however, those theories only cover simplest experimental arrangements, in which the fast particle emerging from the target enters a single large detector measuring only one of the numbers characterizing the particle motion at the expense of erasing the rest of the information.

Modern thin detectors, easily penetrable by fast charged particles and connectable into coincidence schemes, allow more detailed reconstruction of the particle motion history, even if its deflection angles and relative energy losses are small. For instance, a target made of a semiconductor material can serve as an *in situ* detector of ionization energy losses, while the particle incidence and emergence angles can be measured in the same event by a few thin pixelized plates placed upstream and downstream the target (a “telescope”). For such advanced setups, Molière and Landau theories do not describe all the features of the particle distribution, inasmuch as they do not bring out possible correlation between the deflection angle and the energy loss. There thus arises a need to evaluate the two-variable probability distribution function, involving the correlation. It may also be used for a variety of applied problems, such as calculation of 3d spatial distribution of stopped particles (see [7] and refs. therein), or ionization loss control of channeling states and dechanneling rates in crystals [11], etc.

Specific mechanisms of angle-energy loss correlation depend on the particle energy. Historically the first kind

thereof, being due to the curvature extension of the particle path (“detour”) in a slab target, increasing with the increase of the emergence angle, was predicted in [12, 13]. Since correlation of this kind is quadratic in the particle deflection angles, and thus inversely proportional to the large particle momentum squared, it becomes negligible at high energy.

Another correlation mechanism is due to sampling a higher electron density by particles passing near atomic nuclei, where the deflecting Coulomb field is stronger, too [14–17]. It is pertinent to slow ($\lesssim 100$ keV) ions, when the ionization process is semiclassical. Confronting the single-collision mean energy loss $\Delta\epsilon(r_{\perp})$ as a function of the impact parameter r_{\perp} wrt to the atomic nucleus [11], and single-collision deflection angle $\chi(r_{\perp})$, one infers the elementary correlation between $\Delta\epsilon$ and χ . With the increase of the light ion energy, the semiclassical character of the scattering process eventually gets violated, but experimentally, the correlation was found to persist out to MeV ion energies [18, 19], where all the above mentioned mechanisms, as well as nonuniformity of the target thickness [24], seem to be not enough to explain the data [11, 20, 21].

At sufficiently high energies, when both scattering and ionization processes are quantum mechanical, it becomes more appropriate to compare relative contributions from different correlation mechanisms by counting the minimal necessary number of interactions of the fast charged particle with electrons and nucleus within one atom in the medium. The above mentioned correlation of the electron density with the location of the deflecting atomic nucleus requires at least a two-photon exchange, in which one photon is exchanged with the static but highly charged nucleus, causing deflection of the incident charged particle, while another photon is exchanged with the knocked-out electron, transferring it energy. But a positive correlation must exist even at the one-photon exchange level, when a virtual photon knocks out an atomic electron, imparting it energy and transverse momentum simultaneously. That mechanism, being of the lowest order in the electron charge, should ultimately dominate at high

*Electronic address: bon@kipt.kharkov.ua

energy.

Besides comparing different effects in single scattering, it is important to take into account that targets for high-energy particles are usually made sufficiently thick. The correlation may then be attenuated by multiple interactions with different atoms. In this regard, it is crucial that Coulomb scattering of point-like charged particles permits significant momentum transfers in single scatterings, contributing both to Rutherford “tails” at large deflection angles, and to an anomalous (logarithmically modified) diffusion at typical angles. That does not conflict with the dominance of the single-photon exchange in the correlation.

In application to high-energy charged particle passage problems, it is thus important to investigate angle-energy loss correlation induced by scattering of the projectile on individual atomic electrons (hard incoherent scattering). This effect must be the strongest for relativistic incident electrons or positrons, because they have the same mass as the struck electrons, and thus can transfer them a large fraction of energy in “head-on” collisions. As for the target materials, more favourable should be low- Z ones, for which the relative role of incoherent scattering is large.

The present paper aims to calculate the hard incoherent type of angle-energy loss correlation for multiple scattering of relativistic electrons or positrons in low- Z amorphous matter. This process is governed by a spatially uniform transport equation, solvable by conventional integral transformation techniques (Sec. II). In the multiple scattering regime, the solution can make use of the same logarithmic approximations as in Molière, Fano, and Landau theories. It proves that for characterization of the substance, there is no need to introduce phenomenological parameters other than the elastic and inelastic screening angles χ_a and χ_{in} , and the mean excitation energy I_δ , including the density correction δ . Furthermore, I_δ only contributes to an overall shift in the mean energy loss (just like for Landau distribution), whereas χ_a and χ_{in} coalesce into a single parameter. Our next task is to investigate the distribution function dependence on the two kinematic variables characterizing the final electron, and on two parameters (Z and thickness) characterizing the target. We find (Secs. III–V) that the correlation remains substantial even in thick targets, but its origin is different from that for mechanisms alluded above (extension of the path, impact parameter mediated correlation, etc.). We will also study the correlation in terms of partial mean values taken with the two-variable distribution function (Sec. VI).

II. SOLUTION OF THE TRANSPORT EQUATION

The correlated process of small-angle scattering of a fast electron on atoms of an amorphous substance, and of the associated energy loss, may be described by a trans-

port equation

$$\frac{\partial}{\partial l} f(\boldsymbol{\theta}, \epsilon, l) = -n_a \int d\sigma_{el}(\chi) [f(\boldsymbol{\theta}, \epsilon, l) - f(\boldsymbol{\theta} - \boldsymbol{\chi}, \epsilon, l)] - n_a \iint d\sigma_{in}(\chi, \Delta\epsilon) [f(\boldsymbol{\theta}, \epsilon, l) - f(\boldsymbol{\theta} - \boldsymbol{\chi}, \epsilon - \Delta\epsilon, l)], \quad (1)$$

where the first line comprises contributions from elastic collisions, whereas the second line, from inelastic ones (atom excitation or knock-out of an atomic electron). Here f stands for the probability distribution function depending on the fast electron cumulative deflection angle $\boldsymbol{\theta}$ and cumulative ionization energy loss ϵ , and normalized by $\int d^2\theta d\epsilon f = 1$. $d\sigma_{el}$ and $d\sigma_{in}$ are the elastic and inelastic scattering differential cross-sections depending on the single-scattering deflection angle $\boldsymbol{\chi}$ and energy transfer $\Delta\epsilon$. Also, l designates the length traversed in the target, and n_a the density of atoms. It is presumed that $\theta \ll 1$, and ϵ is much smaller than the fast particle energy E , wherewith $d\sigma_{el}$, $d\sigma_{in}$ virtually do not depend on E , as in Molière and Landau theories.

Transport equation (1) is complemented by an initial condition

$$f(\boldsymbol{\theta}, \epsilon, 0) = \delta(\boldsymbol{\theta})\delta(\epsilon),$$

corresponding to a monokinetic initial beam. The solution of this problem is obtained as usual, by applying Fourier and Laplace transformations, which reduce (1) to a 1st-order ordinary linear differential equation, solved by an exponential $e^{-l\kappa(\mathbf{b}, s)}$, where¹

$$\kappa(\mathbf{b}, s) = n_a \int d\sigma_{el}(\chi) (1 - e^{-i\mathbf{b}\cdot\boldsymbol{\chi}}) + n_a \iint d\sigma_{in}(\chi, \Delta\epsilon) \left(1 - e^{-i\mathbf{b}\cdot\boldsymbol{\chi} - 2mp^{-2}s\Delta\epsilon}\right) \quad (2)$$

(\mathbf{b} - and s -factorization). The inverse transformation yields

$$\frac{p^2}{2m} f(\boldsymbol{\theta}, \epsilon, l) = \frac{1}{(2\pi)^2} \int d^2b \times \frac{1}{2\pi i} \int_{-i\infty}^{i\infty} ds e^{i\mathbf{b}\cdot\boldsymbol{\theta} + 2mp^{-2}s\epsilon} e^{-l\kappa(\mathbf{b}, s)}. \quad (3)$$

A factor $2mp^{-2}$, where m and p are the electron mass and momentum (which, just like E , degrades negligibly with the increase of l), has been introduced in Eqs. (2), (3) for further convenience, in order to render s dimensionless and commensurable with b^2 . Granted that neither

¹ Our b variable corresponds to η in Molière’s work [1, 3], while our $2mp^{-2}s$ is designated as p in Landau’s paper [2]. But we reserve p for notation of the momentum, while η , in conjunction with y , for reduced b^2 (see below). The rest of our notations are conventional.

$d\sigma_{el}$ nor $d\sigma_{in}$ depend on the χ azimuth, the latter integrates over, yielding the zero-order Bessel function of the product of $b = |\mathbf{b}|$ and $\chi = |\boldsymbol{\chi}|$:

$$\begin{aligned} \kappa(b, s) &= n_a \int d\sigma_{el}(\chi) [1 - J_0(b\chi)] \\ &+ n_a \iint d\sigma_{in}(\chi, \Delta\epsilon) \left[1 - J_0(b\chi)e^{-2mp^{-2}s\Delta\epsilon}\right]. \end{aligned} \quad (4)$$

At the present, most general level, the 2-variable dependence $d\sigma_{in}(\chi, \Delta\epsilon)$ takes account of all the effects, which can give rise to an angle-energy loss correlation. Which of them survives under conditions of multiple scattering is to be determined next.

a. Multiple-scattering approximation In general, $d\sigma_{el}$ and $d\sigma_{in}$ are complicated functions of χ and $\Delta\epsilon$, reflecting the shell structure of atoms, and possibly even their binding effects in the solid. But under the conditions of multiple scattering, the cumulative θ and ϵ are much greater than typical contributing χ and $\Delta\epsilon$ in the single-scattering cross-sections. Given that $\theta \sim b^{-1}$ and $\epsilon \sim \frac{p^2}{2ms}$, arguments $b\chi$ and $2mp^{-2}s\Delta\epsilon$ of functions in (4) are typically small, so, the differences $1 - J_0(b\chi)$ and $1 - J_0(b\chi)e^{-2mp^{-2}s\Delta\epsilon}$ may be expanded in them to the leading orders:

$$1 - J_0(b\chi) \simeq \frac{b^2}{4}\chi^2, \quad (5)$$

$$1 - J_0(b\chi)e^{-2mp^{-2}s\Delta\epsilon} \simeq \frac{b^2}{4}\chi^2 + 2mp^{-2}s\Delta\epsilon. \quad (6)$$

However, straightforward application of such a procedure under conditions of Coulomb scattering leads to a logarithmic divergence of the integral, as long as both the elastic and inelastic differential scattering cross-sections at large χ obey Rutherford asymptotics:²

$$n_a l d\sigma_{el}(\chi) \underset{\chi \gg \chi_a}{\simeq} n_a l d\sigma_{Ruth}(\chi) = 2Z^2 \bar{\chi}_c^2 \frac{d\chi}{\chi^3}, \quad (7)$$

$$n_a l d\sigma_{in}(\chi, \Delta\epsilon) \underset{\chi \gg \chi_a}{\simeq} 2Z \bar{\chi}_c^2 \frac{d\chi}{\chi^3} d\Delta\epsilon \delta\left(\Delta\epsilon - \frac{p^2}{2m}\chi^2\right), \quad (8)$$

where Ze is the atom nucleus charge, and factor [25]

$$\bar{\chi}_c^2 = \frac{4\pi e^4 n_a l}{p^2 v^2} \quad (9)$$

(with v being the particle velocity), common both for elastic and inelastic processes, includes all the dependencies on the properties of the target except Z . Note that Z -dependence of the elastic scattering contribution (7) is quadratic, due to its coherent nature, whereas inelastic scattering (8) is incoherent, thus being proportional to the number Z of electrons in the atoms. Direct implementation of asymptotics (8) is the distinguishing feature of our approach.

To treat the logarithmically diverging integrals accurately, one needs to proceed to the next-to-leading logarithmic accuracy (NLLA). The standard procedure thereof is to break the semiinfinite χ integration interval by an intermediate χ_1 , such that $\chi_a, \chi_{in} \ll \chi_1 \ll \bar{\chi}_c$, and treat the large- χ contribution more rigorously [beyond expansions (5), (6)], whereas the small- χ contribution – phenomenologically [beyond Rutherford asymptotics (7), (8)].

b. Soft scattering contribution In the inner region $\chi < \chi_1$, expansions (5), (6) may be used safely. The deviation from logarithmic χ_1 -dependencies of the integrals are incorporated in the NLLA in terms of the definition

$$d\sigma_{el} = \mathbf{q}(Z, p\chi/\hbar) d\sigma_{Ruth}, \quad \mathbf{q}(Z, \infty) = 1, \quad \mathbf{q}(Z, 0) = 0, \quad (10)$$

$$\int_0^{\chi_1} \mathbf{q}\left(Z, \frac{p\chi}{\hbar}\right) \frac{d\chi}{\chi} = \ln \frac{\chi_1}{\chi'_a} + \gamma_E - 1 \quad (11)$$

for the elastic scattering function \mathbf{q} and the Molière's screening angle $\chi'_a(Z)$ [1, 3],³ similar definition

$$\int_0^\infty d\Delta\epsilon \frac{d\sigma_{in}}{d\Delta\epsilon d\chi} = \frac{d\sigma_{in}}{d\chi} = \mathbf{S}\left(Z, \frac{p\chi}{\hbar}\right) \frac{d\sigma_{Ruth}}{d\chi}, \quad (12)$$

$$\int_0^{\chi_1} \mathbf{S}\left(Z, \frac{p\chi}{\hbar}\right) \frac{d\chi}{\chi} = \ln \frac{\chi_1}{\chi'_{in}} + \gamma_E - 1 \quad (13)$$

² In treatment of electron scattering on atomic nuclei, we neglect nuclear size effects [22] and spin corrections at wide scattering angles [23]. In contrast to the primary electron, knocked-out electrons in (8) are regarded as non-relativistic, wherewith their dispersion law is $\Delta\epsilon = \frac{p^2 \chi^2}{2m}$. As in the case of the Landau distribution, that is sufficient for description of the straggling far from the upper end of its spectrum.

³ Following the notation of [3], the prime at χ'_a , discriminates it from the unprimed value $\chi_a = \chi'_a e^{1/2 - \gamma_E}$, whose advantage is that it coincides with the inverse screening radius times p^{-1} for Born scattering in a pure Yukawa potential [1]. But since Yukawa potential is rather artificial in atomic physics, not being realized even for hydrogen atom, we work from the outset with the primed notations, in which the final results will have the simplest structure. Similar relationship is implied for χ'_{in} .

for the inelastic scattering function S and the corresponding Fano angle $\chi'_{in}(Z)$ [25],⁴ and

$$\iint_{\chi < \chi_1} d\sigma_{in} \Delta\epsilon = \frac{4\pi Z e^4}{m v^2} \left(\ln \frac{p\gamma\chi_1}{I_\delta} - \frac{v^2}{2c^2} \right), \quad (15)$$

$$\ln I_\delta = \ln I + \frac{1}{2}\delta \quad (16)$$

for the mean excitation energy $I(Z)$ (see [26] and refs. therein), and density correction $\delta(Z, \gamma)$ in (16) accounts for dispersive dielectric susceptibility of the medium [8].⁵ Combined, that gives

$$\begin{aligned} n_a l \int_0^{\chi_1} d\chi \frac{d\sigma_{el}}{d\chi} [1 - J_0(b\chi)] &\simeq n_a l \frac{b^2}{4} \int_0^{\chi_1} d\chi \frac{d\sigma_{el}}{d\chi} \chi^2 \\ &= \frac{Z^2 \bar{\chi}_c^2 b^2}{2} \left(\ln \frac{\chi_1}{\chi'_a} + \gamma_E - 1 \right), \end{aligned} \quad (17)$$

$$\begin{aligned} n_a l \iint_{\chi < \chi_1} d\sigma_{in} [1 - J_0(b\chi) e^{-2mp^{-2}s\Delta\epsilon}] \\ \simeq n_a l \frac{b^2}{4} \iint_{\chi < \chi_1} d\sigma_{in} \chi^2 + 2mp^{-2} n_a l s \iint_{\chi < \chi_1} d\sigma_{in} \Delta\epsilon \\ = 2Z \bar{\chi}_c^2 \left[\frac{b^2}{4} \left(\ln \frac{\chi_1}{\chi'_a} + \gamma_E - 1 \right) + s \left(\ln \frac{p\gamma\chi_1}{I_\delta} - \frac{v^2}{2c^2} \right) \right]. \end{aligned} \quad (18)$$

Notably, this part does not yield any angle-energy loss correlation, including that mentioned in the Introduction (sampled higher electron density in the regions of stronger deflecting field near the nucleus). The reason is that this contribution is concentrated at limited energy and momentum transfers, but the lowest-order expansion in their Fourier-reciprocal variables involves no cross terms. If the diffusion was normal, that would be the end of the story for thick targets.

⁴ Assuming electrons to be relativistic and target's Z to be low or moderate, here we will neglect Coulomb corrections, i.e., the cross-section dependence on $Z e^2 / \hbar v$. Then, constants χ_a and χ_{in} are determined by atomic formfactors. For their evaluation at low Z , Thomas-Fermi model is too crude, and Hartree-Fock calculations are mandatory [27]. In particular, for hydrogen, $\ln \chi_{in} / \chi_a = \int_0^\infty \frac{d\chi}{\chi} (\mathbf{q} - S) = -5/6$, wherewith $\chi_{in} = e^{-5/6} \chi_a \approx 0.4 \chi_a$, $p\chi_{at} / \hbar = 2 / ea_B$,

$$\frac{p\chi'_{at}}{\hbar} = \frac{p\chi_{at}}{\hbar} e^{\gamma_E - 1/2} = \frac{2}{a_B} e^{\gamma_E - 3/2} \quad (14)$$

[with χ'_{at} defined by Eq. (28) below].

⁵ At $\gamma \rightarrow \infty$, the behavior of $\delta(Z, \gamma)$ is such that

$$\ln \frac{p}{I_\delta} = \ln \frac{m}{\hbar \omega_p(Z)} + \frac{1}{2},$$

where $\omega_p = \sqrt{4\pi Z e^2 n_a / m}$ is the plasma frequency, so, $\delta/2$ and $\ln \gamma$ compensate each other, and the logarithmic growth in Eq. (15) halts.

c. Hard scattering contribution There exists, however, an equally important contribution from the outer region $\chi > \chi_1$. For its treatment, it is justified to apply Rutherford asymptotics (7), (8), but the integrals need to be evaluated without resorting to expansions (5), (6):

$$n_a l \int_{\chi_1}^\infty d\sigma_{el} [1 - J_0(b\chi)] \simeq 2Z^2 \bar{\chi}_c^2 \int_{\chi_1}^\infty \frac{d\chi}{\chi^3} [1 - J_0(b\chi)], \quad (19)$$

$$\begin{aligned} n_a l \iint_{\chi > \chi_1} d\sigma_{in} [1 - J_0(b\chi) e^{-s\chi^2}] \\ \simeq 2Z \bar{\chi}_c^2 \int_{\chi_1}^\infty \frac{d\chi}{\chi^3} [1 - J_0(b\chi) e^{-s\chi^2}]. \end{aligned} \quad (20)$$

Integral (19) is exactly the same as that arising in the Bethe-Molière theory, with the known result

$$\int_{\chi_1}^\infty \frac{d\chi}{\chi^3} [1 - J_0(b\chi)] \underset{b\chi_1 \rightarrow 0}{\simeq} \frac{b^2}{4} \left(\ln \frac{2}{b\chi_1} + 1 - \gamma_E \right). \quad (21)$$

Integral (20) is somewhat more sophisticated, and is evaluated in Appendix A:

$$\begin{aligned} \int_{\chi_1}^\infty \frac{d\chi}{\chi^3} [1 - J_0(b\chi) e^{-s\chi^2}] \underset{b\chi_1, s\chi_1^2 \rightarrow 0}{\simeq} \frac{b^2}{4} + \frac{s}{2} e^{-b^2/4s} \\ - \frac{1}{2} \left(s + \frac{b^2}{4} \right) \left[\ln s\chi_1^2 + \gamma_E + \text{Ein} \left(\frac{b^2}{4s} \right) \right], \end{aligned} \quad (22)$$

with Ein the complementary exponential integral function specified by Eq. (A6). Again, the χ_1 -dependence here is simple logarithmic. As for b and s dependencies, in contrast to Eqs. (17), (18), they get intermixed. It is this mixing that gives rise to a correlation between θ and ϵ .

d. Combined result Ultimately, piecing together (21) with (17), and (22) with (18), we cancel the delimiting parameter χ_1 , and are left with

$$\begin{aligned} l\kappa(b, s) = Z \bar{\chi}_c^2 \left\{ \frac{b^2}{2} \left(Z \ln \frac{2}{b\chi'_a} + \ln \frac{1}{\chi'_{in}} + \gamma_E \right) \right. \\ \left. + s \left(2 \ln \frac{p\gamma}{I_\delta} + e^{-b^2/4s} - \frac{v^2}{c^2} \right) \right. \\ \left. - \left(s + \frac{b^2}{4} \right) \left[\ln s + \gamma_E + \text{Ein} \left(\frac{b^2}{4s} \right) \right] \right\}. \end{aligned}$$

The final integral can be written more compactly by changing b and s to reduced integration variables

$$y = Z^2 \bar{\chi}_c^2 b^2, \quad u = Z \bar{\chi}_c^2 s, \quad (23)$$

which absorb the energy dependence and simplify the thickness dependence. Accordingly, kinematic variable θ is changed to

$$\Theta = \frac{\theta}{Z \bar{\chi}_c}, \quad (24)$$

and ϵ to

$$\lambda(Z, l, \epsilon) = \frac{2m}{p^2 Z \bar{\chi}_c^2} \epsilon - \ln \frac{p^2 \gamma^2 Z \bar{\chi}_c^2}{I_\delta^2} + \gamma_E - \gamma^{-2}, \quad (25)$$

with an additional shift arising after combining the term ϵu in the exponent with other terms linear in u . In these notations, the distribution function express as

$$\begin{aligned} \frac{p^2}{2m} Z^3 \bar{\chi}_c^4 f(Z, l, \theta, \epsilon) &= F(Z, y_0, \Theta, \lambda) \\ &= \frac{1}{4\pi} \int_0^{y_{\max}} dy J_0(\sqrt{y}\Theta) e^{\Omega_{el}(y_0, y)} \\ &\quad \times \frac{1}{2\pi i} \int_{-i\infty}^{i\infty} du e^{\lambda u + \Omega_{in}(y/4Z, u)}, \quad (26) \end{aligned}$$

with

$$y_0(l, Z) = 4Z \left(\frac{Z \bar{\chi}_c^2}{\chi_{at}^2} \right)^{1+1/Z} e^{\gamma_E/Z} \gg 1, \quad (27)$$

$$\chi'_{at} = \chi'_a \frac{Z}{Z+1} \chi'_{in} \frac{1}{Z+1}, \quad (28)$$

$$\Omega_{el}(y_0, y) = -\frac{y}{4} \ln \frac{y_0}{y}, \quad (29)$$

$$\Omega_{in}(Y, u) = (u + Y) [\ln u + \text{Ein}(Y/u)] + u \left(1 - e^{-Y/u} \right). \quad (30)$$

Functions (29), (30) are defined so that they vanish at the origin: $\Omega_{el}(y_0, 0) = \Omega_{in}(0, 0) = 0$. As can be verified with the use of identities

$$\int_{-\infty}^{\infty} d\lambda \frac{1}{2\pi i} \int_{-i\infty}^{i\infty} du e^{\lambda u + \Omega_{in}(Y, u)} = e^{\Omega_{in}(Y, 0)}, \quad (31)$$

$$\int_0^{\infty} d\Theta \Theta \int_0^{\infty} dy J_0(\sqrt{y}\Theta) e^{\Omega_{el} + \Omega_{in}} = 2e^{\Omega_{el} + \Omega_{in}} \Big|_{y=0} \quad (32)$$

(being particular cases of inverse Fourier and Fourier-Bessel transformations), F is normalized to unity in variables Θ and λ :

$$2\pi \int_0^{\infty} d\Theta \Theta \int_{-\infty}^{\infty} d\lambda F(Z, y_0, \Theta, \lambda) = 1,$$

in accordance with its interpretation as a probability density.

Before proceeding, let us analyze the structure of the obtained integral (26). Even though one of its entries, Ω_{in} , looks somewhat cumbersome, involving a special function Ein , its second u -derivative is very simple:

$$\frac{\partial^2}{\partial u^2} \Omega_{in}(Y, u) = \frac{1}{u} e^{-Y/u}. \quad (33)$$

[This relation can be derived directly by double differentiating (22) over s , and setting thereupon $\chi_1 = 0$, owing

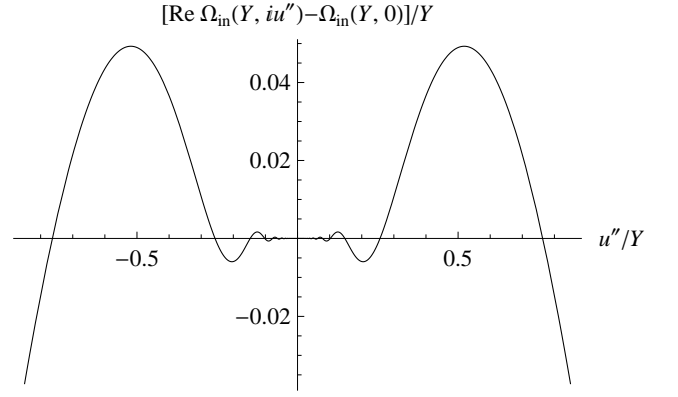


FIG. 1: The real part of $\Omega_{in}(Y, iu'') - \Omega_{in}(Y, 0)$, with Ω_{in} defined by Eq. (30), for real u'' and Y .

to the convergence of the integral at the upper limit.] We will take advantage of property (33) below.

Next, it is worth noting that besides the dependence of the exponent $\Omega_{el} + \Omega_{in}$ on variables y and u , in terms of which the transport equation has been factorized, it depends on parameters Z and y_0 . In total, that amounts to a 4-variable dependence, but in Eq. (26) it actually splits into a sum of two functions, each depending only on two variables. This does not guarantee any strict factorization of the resulting Fourier integral yet, insofar as both Ω 's depend on y . After the integration over y , the dependencies on Θ and λ get intermixed. In this regard, it is worth reminding that y is a rescaled square of \mathbf{b} [Eq. (23)], where \mathbf{b} may be regarded as an analogue of an impact parameter. The correlation between Θ and λ may then be interpreted as being due to correlations of each of them with \mathbf{b} , so that the mentioned property is akin to impact-parameter-mediated correlation for slow ions (cf. Introduction). It should be understood, however, that \mathbf{b} is not a physical transverse coordinate \mathbf{r}_\perp , being just a Fourier reciprocal to $\boldsymbol{\theta}$ at the probability level.

The dependence of Ω_{in} on y and Z only though their ratio reflects the fact that aggregate scattering on atomic electrons, due to its incoherence, is Z times weaker than on atomic nuclei. (Recall that a coherent scattering factor Z^2 has been included in the definition of y , while incoherent scattering factor Z , in the definition of u .) Besides that, Ω_{in} involves functions depending only on the ratio y/Zu . As we will see in Sec. IV, this implies asymptotic dependence only on the ratio of λ and Z .

To decide whether Eq. (26) is suitable for numerical evaluation, it is also necessary to assess the rate of convergence of its integrals. The u -dependence of the integrand is determined by Ω_{in} . Therein, $\text{Ein}(Y/u) \xrightarrow{|u| \rightarrow \infty} 0$, hence,

at imaginary integration variable $u = iu''$ and large $|u''|$, Ω_{in} behaves as $\Re e(u \ln u) = -\frac{\pi}{2}|u''|$, linearly tending to $-\infty$. Hence, at infinity the u -integral converges exponentially, which is rapid enough. On the other hand, in the limit of small imaginary u , functions $e^{-Y/u}$ and $\text{Ein}(Y/u)$ rapidly oscillate, and even though the exponent at that

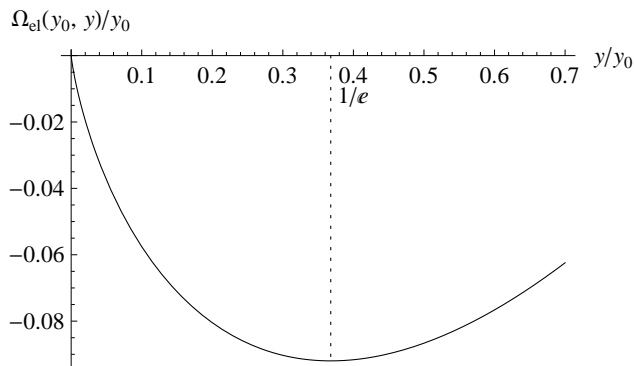


FIG. 2: The behavior of $\Omega_{el}(y_0, y)$ defined by Eq. (29). Dotted line indicates the location of its maximum, which is the upper limit for y_{\max}/y_0 .

does not blow up (see Fig. 1), it may be expedient to introduce a small lower cutoff, e.g., $|u''|_{\min} \sim 10^{-5}$.

As for the y -integral in Eq. (26), it is primarily determined by the behavior of Ω_{el} . In the limit $y \rightarrow 0$, both Ω_{el} and Ω_{in} are finite, but Ω_{el} begins to grow when $y > y_0/e$ (see Fig. 2), threatening with a divergence of the entire integral. Just like in the Molière theory, that is merely an artifact of the small- y approximation, to avoid which, it suffices to introduce a sizable upper cutoff y_{\max} , being not larger than $\sim y_0/e$:

$$1 \ll y_{\max} \lesssim y_0/e$$

The result of the integration is then insensitive to y_{\max} . At that, given that $|\Omega_{el}| < 0.08 y_0$ (see Fig. 2), the necessary condition for the target to be physically thick ($|\Omega_{el}| \gg 1$) is

$$y_0 \gtrsim 10^2.$$

To give an idea of numerical values of the reduced target thickness y_0 used in further examples, Table I lists parameters of several low- Z targets corresponding to a few exemplary y_0 .

TABLE I: Reduced thickness y_0 for ultrarelativistic electrons, neglecting Coulomb corrections, based on atomic elastic scattering formfactors and inelastic scattering functions tabulated in [28].

Z	$p\chi'_{at}/\hbar$	$y_0 = 10^2$	$y_0 = 10^4$	$y_0 = 10^6$
1	1.50 \AA^{-1}	$l = 0.28 \frac{\text{mg}}{\text{cm}^2}$	$l = 2.82 \frac{\text{mg}}{\text{cm}^2}$	$l = 28.2 \frac{\text{mg}}{\text{cm}^2}$
2	2.91 \AA^{-1}	$l = 2.29 \frac{\text{mg}}{\text{cm}^2}$	$l = 49.3 \frac{\text{mg}}{\text{cm}^2}$	$l = 1.06 \frac{\text{g}}{\text{cm}^2}$
3	3.10 \AA^{-1}	$l = 51.5 \mu\text{m}$	$l = 1.63 \text{ mm}$	$l = 5.15 \text{ cm}$
4	3.44 \AA^{-1}	$l = 15.6 \mu\text{m}$	$l = 0.62 \text{ mm}$	$l = 2.47 \text{ cm}$
5	3.75 \AA^{-1}	$l = 11.3 \mu\text{m}$	$l = 0.526 \text{ mm}$	$l = 2.44 \text{ cm}$
6	3.88 \AA^{-1}	$l = 12.63 \mu\text{m}$	$l = 0.651 \text{ mm}$	$l = 3.37 \text{ cm}$

III. COMPUTED DISTRIBUTIONS

Examples of the computed density plots in the Θ - λ plane are presented in Figs. 3a, 4a. Their typical structure is an elliptic concentration at moderate λ , Θ (formed in the process of multiple scattering), and a “spur” along a parabola

$$\lambda = Z\Theta^2, \quad (34)$$

extending to higher λ and Θ (being due to single hard scattering). The oblique orientation of the latter feature is an unambiguous indication that the distribution does not reduce to a product of a Θ -dependent distribution and a λ -dependent one. At a closer examination, we observe that when the spur merges with the dominant central spot, it somewhat squeezes the latter. Inspection of projections of those distributions onto Θ and λ axes (Figs. 3b,c, 4b,c, 5, 6) further reveals that their shapes are qualitatively similar to Landau and Molière distributions (cf. Figs. 7, 8 below), but the width of the Θ distribution depends on λ and vice versa. At sufficiently large λ , the projected Θ -distribution can develop a second maximum (a slice of the spur – see Figs. 3b,c, 4b).

The two-component structure of the probability distribution hints that in the corresponding regions, the double Fourier integral representation (26) may admit some additional approximations. But in any case, the description of F can not be simpler than that of its single-variable (λ or Θ) projections, which are Landau and Molière distributions, known to be irreducible to elementary functions. The intrinsic simplicity of the latter owes instead to their stability properties, i.e., invariance with respect to convolution, as exemplified by Eq. (37) below. By virtue of that, Landau and Molière distributions can actually serve as building blocks even in the two-variable case. It will be not superfluous to briefly remind their basic properties.

A. Landau distribution

Integration of Eq. (26) over the full Θ plane can be done with the aid of identity (32), and results in

$$\begin{aligned} & 2\pi \int_0^\infty d\Theta \Theta F(Z, y_0, \Theta, \lambda) \\ &= \frac{1}{2\pi i} \int_{-i\infty}^{i\infty} du e^{\lambda u + \Omega_{in}(0, u)} = \varphi_L(\lambda). \end{aligned} \quad (35)$$

Here

$$\Omega_{in}(0, u) = u \ln u, \quad (36)$$

so, φ_L is recognized to be the Landau distribution [2, 29]. It is normalized by

$$\int_{-\infty}^\infty d\lambda \varphi_L(\lambda) = e^{\Omega_{in}(0,0)} = 1,$$

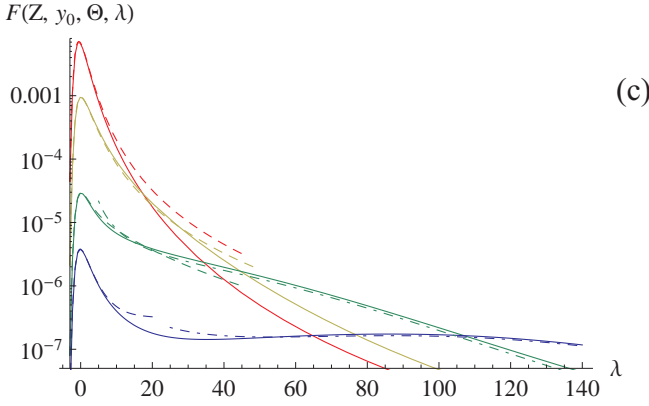
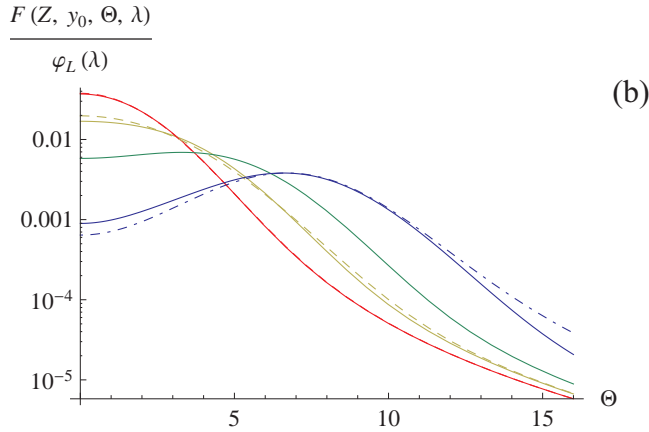
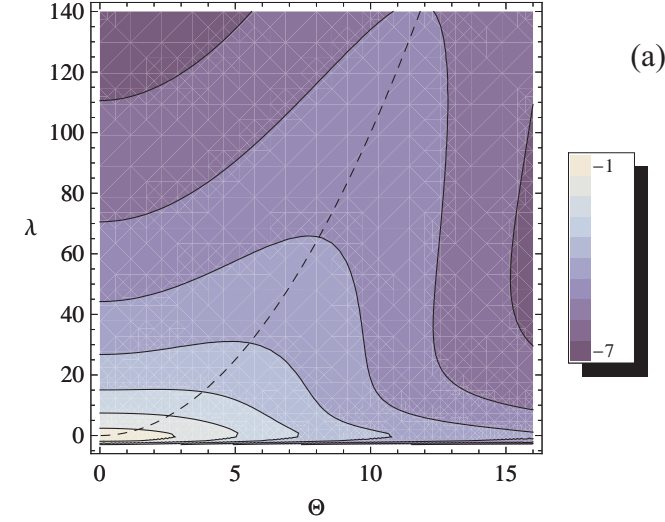


FIG. 3: Correlated angle-energy loss distribution of electrons multiple scattered in hydrogen ($Z = 1$) target of reduced thickness $y_0 = 10^4$. a). Contour plot of $\log F$, with F given by Eq. (26). Dashed parabola, $\lambda = Z\Theta^2$. b). Angular distributions at fixed values of the ionization energy loss straggling variable λ . Solid curves, calculation by exact formula (26), at $\lambda = 0$ (red), $\lambda = 7$ (yellow), $\lambda = 20$ (green), $\lambda = 50$ (blue). Dashed, approximation (58). Dot-dashed, approximation (70), (71b). c). Ionization energy loss distribution at fixed values of the scattering angle. Solid curve, $\Theta = 0$ (red), $\Theta = 4$ (yellow), $\Theta = 8$ (green), $\Theta = 16$ (blue). Dashed and dot-dashed curves correspond to the same approximations as in (b).

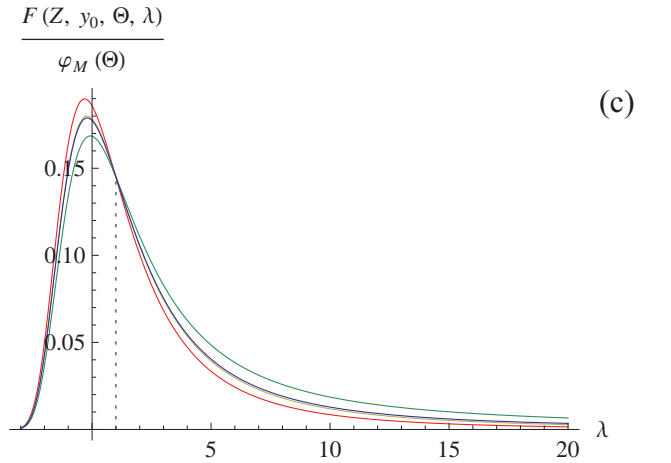
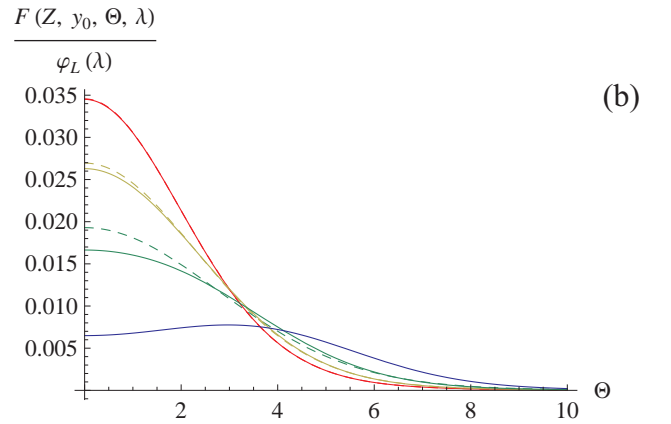
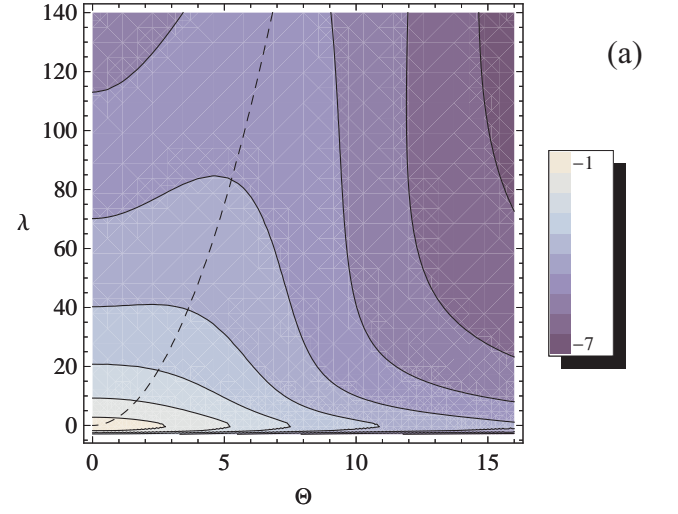


FIG. 4: Correlated angle-energy loss distribution of electrons multiple scattered in lithium ($Z = 3$) target of reduced thickness $y_0 = 10^4$. a). Contour plot of $\log F$, with F given by Eq. (26). Dashed parabola, $\lambda = Z\Theta^2$. b). Angular distributions at fixed values of the ionization energy loss straggling variable λ . Solid curves, calculation by exact formula (26), at $\lambda = 0$ (red), $\lambda = 7$ (yellow), $\lambda = 20$ (green), $\lambda = 50$ (blue). Dashed, approximation (58). Dot-dashed, approximation (70), (71b). c). Ionization energy loss distribution at fixed values of the scattering angle. Solid curve, $\Theta = 0$ (red), $\Theta = 3$ (yellow), $\Theta = 6$ (green), $\Theta = 15$ (blue). In the moderate λ domain, the latter is the closest to Landau distribution. All the straggling curves intersect at $\lambda = 1$ (dotted vertical line).

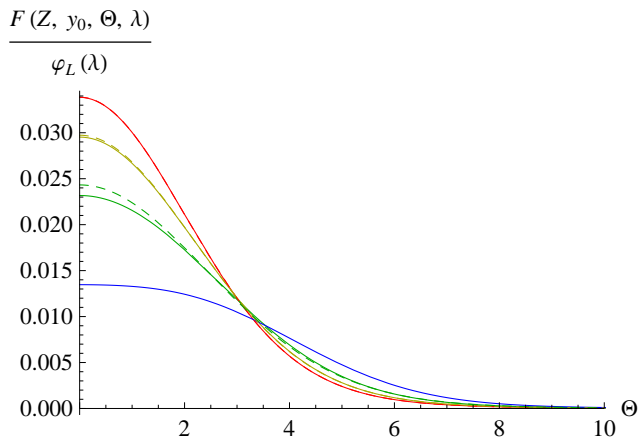


FIG. 5: Angular distributions of electrons multiple scattered in carbon ($Z = 6$) target of reduced thickness $y_0 = 10^4$, at fixed values of the ionization energy loss straggling variable λ : $\lambda = 0$ (red), $\lambda = 7$ (yellow), $\lambda = 20$ (green), $\lambda = 50$ (blue). Solid curves are calculated by exact formula (26). Dashed, approximation (58). Dot-dashed, approximation (70), (71b).

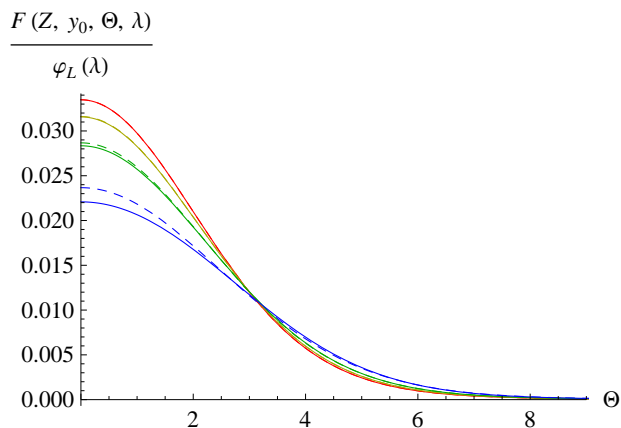


FIG. 6: The same as Fig. 5, for silicon ($Z = 14$) target of reduced thickness $y_0 = 10^4$.

has the group property

$$\int_{-\infty}^{\infty} d\lambda_1 \varphi_L(\lambda_1) \varphi_L(\lambda - \lambda_1) = \frac{1}{2} \varphi_L\left(\frac{\lambda}{2} - \ln 2\right), \quad (37)$$

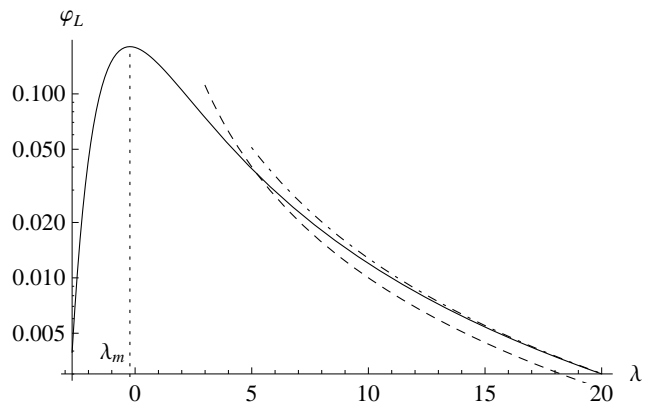


FIG. 7: Log plot of Landau distribution (35) (solid curve). Dashed curve, Rutherford asymptotics (39) (approaching the solid curve at very large λ). Dot-dashed, Rutherford asymptotics with power correction (38), approaching the solid curve more rapidly. The most probable energy loss [Eq. (40)], corresponding to the maximum of φ_L , is marked by the dotted vertical line.

and in the large energy loss region, features a single-scattering, Rutherford symptotics⁶

$$\varphi_L(\lambda) \underset{\lambda \rightarrow \infty}{\simeq} \frac{1}{2\pi i} \int_{-i\infty}^{i\infty} du e^{\lambda u} u \ln u = \frac{1}{\lambda^2}. \quad (39)$$

At $\lambda \rightarrow -\infty$, function $\varphi_L(\lambda)$ drops off faster than exponentially, as can be demonstrated by integration in a saddle-point approximation [2]. The entire shape of $\varphi_L(\lambda)$ is markedly asymmetric (see Fig. 7). Its maximum is achieved at

$$\lambda = \lambda_m \approx -0.22 \quad (40)$$

(the most probable energy loss, MPEL). In this point,

$$\varphi_L(\lambda_m) \approx 0.18, \quad \varphi'_L(\lambda_m) = 0, \quad \varphi''_L(\lambda_m) \approx -0.079. \quad (41)$$

⁶ Asymptotics (39) becomes sufficiently accurate only in a rather remote region (see Fig. 7, dashed curve). Higher accuracy may be achieved by retaining a correction term:

$$\begin{aligned} \varphi_L(\lambda) \underset{\lambda \rightarrow \infty}{\simeq} \frac{1}{2\pi i} \int_{-i\infty}^{i\infty} du e^{\lambda u} \left(u \ln u + \frac{1}{2} u^2 \ln^2 u \right) \\ = \frac{1}{\lambda^2} + \frac{2 \ln \lambda + 2\gamma_E - 3}{\lambda^3} \end{aligned} \quad (38)$$

(displayed in Fig. 7 by the dot-dashed curve). In the present paper, for simplicity, we will restrict our analysis to the leading-order asymptote (39) and its counterparts for the joint distribution function (see Sec. VB). It should be minded that at moderately large λ , their accuracy is limited.

B. Molière distribution

Similarly, integration over λ in (26) proceeds with the use of identity (31), yielding

$$\int_{-\infty}^{\infty} d\lambda F(Z, y_0, \Theta, \lambda) = \frac{1}{4\pi} \int_0^{y_{\max}} dy J_0(\sqrt{y}\Theta) \times e^{\Omega_{el}(y_0, y) + \Omega_{in}(y/4Z, 0)}. \quad (42)$$

Since $\Omega_{in}(y/4Z, 0) = \frac{y}{4Z} (\ln \frac{y}{4Z} + \gamma_E)$ has the same structure as $\Omega_{el}(y_0, y)$ given by Eq. (29), those terms in the exponent may be amalgamated by collecting all the $\ln y + \text{const}$ factors of $-\frac{y}{4}$ as

$$\begin{aligned} \ln \frac{y_0}{y} - \frac{1}{Z} \left(\ln \frac{y}{4Z} + \gamma_E \right) \\ = \frac{Z+1}{Z} \ln \frac{1}{y} + \ln y_0 + \frac{1}{Z} \ln 4Z - \frac{\gamma_E}{Z} \\ = \frac{Z+1}{Z} \ln \frac{4Z^2 \bar{\chi}_c^2}{\chi_{at}^2 y}. \end{aligned} \quad (43)$$

Then, it is expedient to change the integration variable from y to

$$\frac{Z+1}{Z} y = \eta, \quad (44)$$

wherewith the pure angular distribution expresses as

$$\int_{-\infty}^{\infty} d\lambda F(Z, y_0, \Theta, \lambda) = \frac{Z}{Z+1} \varphi_M \left(\frac{4\chi_c^2}{\chi_{at}^2}, \frac{\theta}{\chi_c} \right), \quad (45)$$

where [3]

$$\chi_c^2(Z, l, n_a, p) = Z(Z+1) \bar{\chi}_c^2(l, n_a, p) \equiv \frac{4\pi Z(Z+1) \alpha^2 n_a l}{p^2 v^2} \quad (46)$$

[featuring a $Z(Z+1)$ factor], and

$$\varphi_M(\eta_0, \Psi) = \frac{1}{4\pi} \int_0^{\eta_{\max}} d\eta J_0(\sqrt{\eta}\Psi) e^{-\frac{\eta}{4} \ln \frac{\eta_0}{\eta}} \quad (47)$$

(with $\eta_{\max} \sim y_{\max}$, the sensitivity to which is weak) is the Molière distribution normalized by

$$2\pi \int_0^{\infty} d\Psi \Psi \varphi_M(\eta_0, \Psi) = 1.$$

All the target characteristics Z and l enter here via a single parameter η_0 , whose value in Eq. (45), however, somewhat differs from y_0 defined by Eq. (27). Similarly, variable θ/χ_c somewhat differs from Θ defined by Eq. (24). That may raise a question whether reduced variables y_0 and Θ were chosen most conveniently, but the answer is that whereas variables $\eta_0, \theta/\chi_c$ are natural for the λ -integrated or large- λ distributions, variables y_0 and Θ are the best suited for the two-variable case.

For understanding the behavior of φ_M , it is rewarding to observe that it obeys an ordinary diffusion equation, with $\ln y_0$ playing the role of the “time” variable:

$$\frac{\partial \varphi_M}{\partial \ln y_0} = \frac{1}{4} \Delta_{\Psi} \varphi_M, \quad \Delta_{\Psi} = \frac{\partial^2}{\partial \Psi^2} + \frac{1}{\Psi} \frac{\partial}{\partial \Psi}. \quad (48)$$

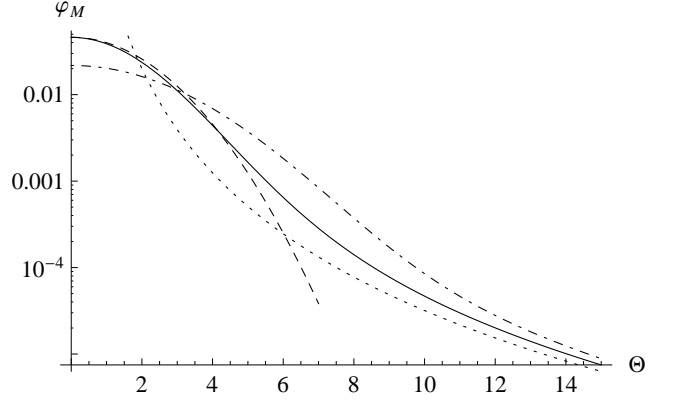


FIG. 8: Log plot of Molière distribution (47) for $\eta_0 = 10^3$ (solid curve). Dashed curve, its LLA (50). Dot-dashed, Molière distribution for $\eta_0 = 10^6$. Dotted curve, Rutherford asymptotics (49), valid for any y_0 .

This equation only describes a hard part of the diffusion, whereas the soft, normal diffusion is contained in the explicit square root dependence of Θ on l [see Eqs. (24), (9)]. In spite of having only a logarithmic thickness dependence, the hard diffusion in a thick target is as significant as the soft one. Yet despite being governed by a normal diffusion equation, φ_M is non-Gaussian in Ψ , insofar as it does not correspond to a $\delta(\Psi)$ initial condition. In particular, for all η_0 it exhibits the same large- Θ Rutherford “tail”

$$\varphi_M(\eta_0, \Psi) \underset{\Psi \rightarrow \infty}{\simeq} \frac{1}{16\pi} \int_0^{\infty} d\eta \ln \eta J_0(\sqrt{\eta}\Psi) = \frac{1}{\pi \Psi^4} \quad (49)$$

(see Fig. 8, dotted curve). It is illegitimate to evolve φ_M back to small $\ln \eta_0$, anyway, because η_0 needs to be kept large in order to ensure negligible dependence of φ_M on the upper integration limit in definition (47). Therewith, the hard diffusion does not reduce to a rescaling of the deflection angle with time.

At $\eta_0 \rightarrow \infty$, the simplest approximation for φ_M is the leading logarithmic (dating back to Williams [6, 30]), when in the exponential entering Eq. (47) $\ln \eta$ is neglected compared to $\ln \eta_0$:

$$\begin{aligned} \varphi_M(\eta_0, \Psi) \underset{\eta_0 \rightarrow \infty}{\simeq} \frac{1}{4\pi} \int_0^{\infty} d\eta J_0(\sqrt{\eta}\Psi) e^{-\frac{\ln \eta_0}{4} \eta} \\ = \frac{1}{\pi \ln \eta_0} e^{-\Psi^2 / \ln \eta_0}. \end{aligned} \quad (50)$$

The accuracy of this Gaussian approximation is illustrated in Fig. 8 by the dashed curve. It can be satisfactory for description of low-statistics experiments in the central angular region, but, as we shall see below, is usually too crude for treatment of angle-energy loss correlation effects.

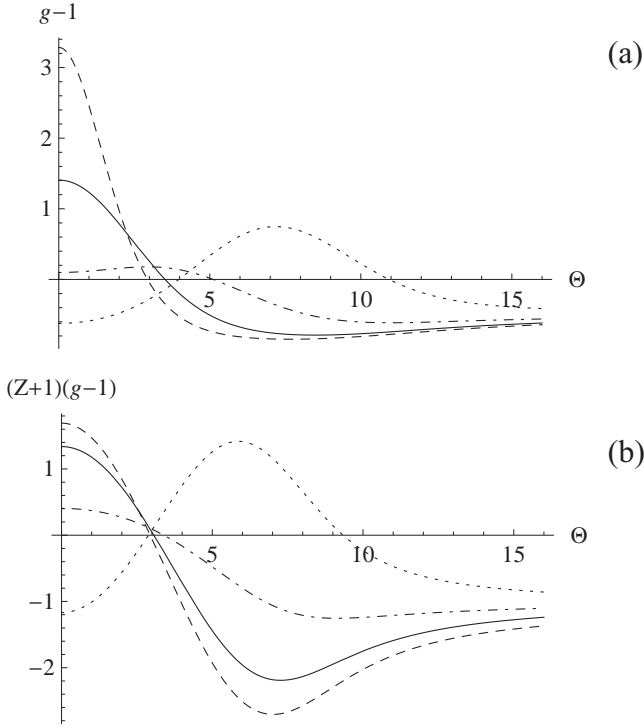


FIG. 9: (a). Deviation of the normalized correlation function Eq. (52) from unity, for $Z = 1$ and $y_0 = 10^4$. Curves, $\lambda = -3$ (dashed), $\lambda = 0$ (solid), $\lambda = 7$ (dot-dashed), $\lambda = 20$ (dotted). (b). $(Z + 1)(g - 1)$ for $Z = 14$ and the same values of y_0 and λ .

C. Normalized correlation function

The single-variable distributions φ_L , φ_M quoted above can be used to formally define the angle-energy loss correlation. According to (35) and (45), the correlation between those variables would be absent if the distribution function factorized into a product of the corresponding single-variable distributions:

$$F \approx \frac{Z}{Z+1} \varphi_L(\lambda) \varphi_M \left(\frac{4\chi_c^2}{\chi_{at}^2}, \frac{\theta}{\chi_c} \right). \quad (51)$$

The relative deviation from this structure, i.e., deviation of the normalized correlation function

$$\begin{aligned} g(Z, y_0, \Theta, \lambda) &= \frac{Z+1}{Z} \frac{F(Z, y_0, \Theta, \lambda)}{\varphi_L(\lambda) \varphi_M \left(\frac{4\chi_c^2}{\chi_{at}^2}, \frac{\theta}{\chi_c} \right)} \\ &\equiv \frac{Z+1}{Z} \frac{F(Z, y_0, \Theta, \lambda)}{\varphi_L(\lambda) \varphi_M \left(\frac{Z+1}{Z} y_0, \sqrt{\frac{Z}{Z+1}} \Theta \right)} \end{aligned} \quad (52)$$

from unity, thus provides a measure of the correlation.

Inspection of Fig. 9, where difference $g - 1$ is plotted vs. Θ , shows that in general, it is nowhere negligible, unless Z is very large. At high Θ , it tends to a negative constant value

$$g - 1 \xrightarrow{\Theta \rightarrow \infty} -\frac{1}{Z+1}, \quad (53)$$

as will be proven in Sec. V A. At low Θ , difference $g - 1$ appears to be of the same order, but its sign depends on the value of λ (see Figs. 9a,b). The physical reason for the correlation to be generally of the order of $\frac{1}{Z+1}$ is that it is caused only by scattering on atomic electrons, whose aggregate contribution is $\sim Z$ times smaller than that from scattering on atomic nuclei. Heuristically, product $(Z + 1)(g - 1)$ for $Z \geq 6$ is nearly Z -independent for all Θ , λ (see Fig. 9b).

It may thus be concluded that the correlation between λ and Θ is significant enough for light materials, including practical cases such as carbon ($Z = 6$) and silicon ($Z = 14$). At the same time, from Figs. 9a,b it is evident that the behavior of the correlation function is rather rich, and deserves more detailed investigation, which will be provided in the next two sections.

IV. MODERATE ENERGY TRANSFERS. LARGE-THICKNESS AND LARGE- Z APPROXIMATIONS

To gain a deeper insight into the structure of the solution, we need to directly scrutinize the behavior of the double integral (26) in different regimes, corresponding to two main probability concentration regions manifest in Figs. 3a, 4a. Each of those regions may be characterized by its own inherent approximations, in which φ_M and φ_L can emerge in a natural way. Let us begin with the simpler case of the central region, where the bulk of the probability resides.

The central region is populated primarily by events consisting of a sequence of many sufficiently probable soft scatterings in a thick target. At derivation of our generic Eq. (26), it was taken into account that under conditions of multiple scattering, typical contributing values of b and s tend to zero with the increase of the target thickness. That has already brought Ω_{el} to a small- y limiting form, although after passage to the reduced variable y , typical values of the latter decrease only logarithmically. As for Ω_{in} , it involves Ein and an exponential function depending on the ratio $y/4Zu$. Since that ratio in turn depends on u , it can be arbitrarily large or small. But if we demand λ to be bounded from above, typical values of u are non-vanishing. Therewith, at typical $y \xrightarrow{y_0 \rightarrow \infty} 0$, typical values of arguments $y/4Zu$ of functions entering Ω_{in} tend to zero. In order to keep track of the correlation, we need to develop Ω_{in} in this ratio to the next-to-leading, 1st order. Utilizing (36) and the value of the derivative

$$\left. \frac{\partial \Omega_{in}}{\partial Y} \right|_{Y=0} = 2 + \ln u, \quad (54)$$

we expand

$$\Omega_{in}(y/4Z, u) \underset{y/4Zu \ll 1}{\simeq} u \ln u + \frac{y}{4Z} (2 + \ln u). \quad (55)$$

Grouping (55) with the rest of the terms in the exponent,

$$\Omega_{el} + \lambda u + \Omega_{in} \simeq \left(-\frac{y}{4} \ln \frac{y_0}{y} + \frac{y}{2Z} \right) + \lambda u + \left(u + \frac{y}{4Z} \right) \ln u,$$

we find that the exponent contains a mixing term $y \ln u$, which, however, has an extremely simple form.

A. Influence of λ on the Θ -distribution

Granted that the mixing term enters with a small factor $1/4Z$, it can be eliminated approximately by applying a relatively small shift of one of the integration variables:

$$u = \tilde{u} - \frac{y}{4Z}.$$

After the corresponding linearization of the term $\tilde{u} \ln u \simeq \tilde{u} \ln \tilde{u} - y/4Z$, variables y and \tilde{u} approximately separate:

$$\Omega_{el} + \lambda u + \Omega_{in} \simeq -\frac{y}{4} \ln \frac{y_0 K}{y} + \lambda \tilde{u} + \tilde{u} \ln \tilde{u}, \quad (56)$$

where we have introduced a notation

$$K(Z, \lambda) = e^{\frac{\lambda-1}{Z}}. \quad (57)$$

Substitution of (56) to double integral (26) brings it to a quasi-factorized form

$$F(Z, y_0, \Theta, \lambda) \approx \varphi_L(\lambda) \varphi_M[y_0 K(Z, \lambda), \Theta], \quad (58)$$

where λ -dependence, besides φ_L , enters yet to the parameter of φ_M . Its validity condition is $\lambda \sim u^{-1} \ll 4Z/y \sim Z \ln y_0$, i.e.,

$$\lambda \ll Z \ln y_0. \quad (59)$$

It should be noted that since in the rhs $\ln y_0 \gg 1$, the exponent of (57) needs not be small. Granted that the rhs in (59) involves a factor of Z , it may as well be regarded as a large- Z limit. At $Z = 1$, condition (59) is fulfilled worse than for higher Z . Accordingly, the accuracy of (58) for $Z = 1$ is somewhat lower, too (see Fig. 12 below).

From comparison of solid and dashed curves in Figs. 3b,c, 4b, it is evident that approximation (58) is satisfactory even for $\lambda \sim Z \ln y_0$, but breaks down at $\lambda \gg Z \ln y_0$, when there develops a peripheral maximum. As for the scaling dependence on $\frac{\lambda-1}{Z}$ in itself, it can hold to a rather good accuracy – see, e.g., Figs. 10 and 12 below.

Structure (58) may seem to be rather cumbersome, but its physical interpretation is straightforward: In the central region, an increase of λ leads to a broadening of the angular distribution, which is equivalent to an effective increase of the electron path length (multiplication of the length parameter y_0 by a λ -dependent factor K). That is reminiscent of the “detour” mechanism mentioned in the Introduction, with the proviso that the trajectory of a high-energy particle remains nearly straight (there is no actual “detour”). The effect, instead, owes to the

increase of relative contribution of events with large energy transfers, and correspondingly with large momentum transfers, with an increase of λ . The mathematical stability of the shape of the Molière distribution ensures that its shape is in principle unaffected by an admixture of harder scattering, which is the reason φ_M appears in Eq. (58). Finally, the fact that in (58) K depends solely on the ratio λ/Z is explained by recalling that λ and Θ are defined so that for the hard contribution $\lambda/Z \sim \Theta^2$ [see Eq. (34)], and the exponential dependence of K on λ/Z owes to $\ln y_0$ serving as a “time” variable for Θ -diffusion [see Eq. (48)].

B. Influence of Θ on the λ -distribution

Formula (58) may be used, conversely, to determine the influence of fixed value of Θ on the λ -distribution. In the point $\lambda = 1$, as Eqs. (58), (57) indicate, ratio $F(Z, y_0, \Theta, 1)/\varphi_M(y_0, \Theta) \approx \varphi_L(1)$ does not depend on Θ , Z , or y_0 at all. Another virtually fixed point is $\lambda \approx -3$, being effectively the leftmost edge of the distribution (see Fig. 4c). In other points, $F(Z, y_0, \Theta, \lambda)/\varphi_M(y_0, \Theta)$ depends, besides λ , on other variables.

As Figs. 3c, 4c, and more clearly Fig. 10 indicate, the increase of Θ induces a *nonmonotonic* variation of location of the point $\lambda_m(\Theta)$, in which $F(\Theta, \lambda)$ as a function of λ reaches its maximum (Θ -dependent MPEL), i.e.,

$$\left. \frac{\partial}{\partial \lambda} F(Z, y_0, \Theta, \lambda) \right|_{\lambda=\lambda_m(\Theta)} = 0.$$

Formally, in the large- Z limit, $\lambda_m(\Theta)$ can be determined by expanding

$$\varphi_L(\lambda) \simeq \varphi_L(\lambda_m) \left[1 + \frac{\varphi_L''(\lambda_m)}{\varphi_L(\lambda_m)} \frac{(\lambda - \lambda_m)^2}{2} \right],$$

$$\varphi_M(y_0 K, \Theta) \simeq \varphi_M(y_0, \Theta) \left[1 + \frac{\lambda - 1}{Z} \frac{\partial \ln \varphi_M}{\partial \ln y_0} \right],$$

and inserting this to Eq. (58):

$$\frac{F(Z, y_0, \Theta, \lambda)}{\varphi_M(y_0, \Theta)} \approx \varphi_L(\lambda_m) \times \left[1 + \frac{\varphi_L''(\lambda_m)}{\varphi_L(\lambda_m)} \frac{(\lambda - \lambda_m)^2}{2} + \frac{\lambda - 1}{Z} \frac{\partial \ln \varphi_M}{\partial \ln y_0} \right]. \quad (60)$$

Differentiating the rhs of (60) by λ and equating to zero, we find

$$\lambda_m(\Theta) = \lambda_m + \frac{1}{Z} \frac{|\varphi_L''(\lambda_m)|}{\varphi_L(\lambda_m)} \frac{\partial \ln \varphi_M(y_0, \Theta)}{\partial \ln y_0}, \quad (61)$$

where $|\varphi_L''(\lambda_m)|/\varphi_L(\lambda_m) \approx 0.44$.

In physical terms, the nonmonotonic behavior of $\lambda_m(\Theta)$ may be understood as follows. At low Θ , the

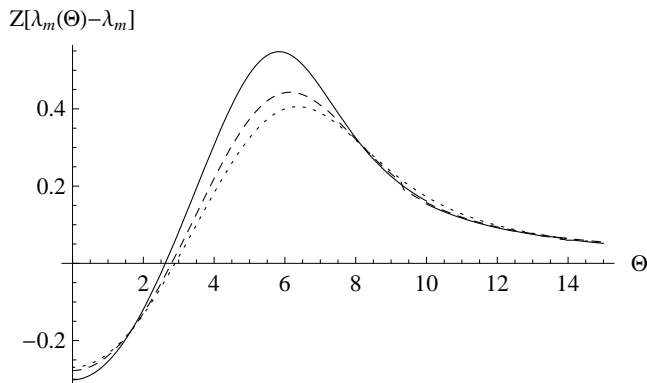


FIG. 10: Θ -dependence of the most probable energy loss [value of λ at which $F(Z, y_0, \Theta, \lambda)$ reaches its maximum wrt λ]. To reduce Z -dependence, the difference $\lambda_m(\Theta) - \lambda_m$ is multiplied by Z . Solid curve, for $Z = 1$; dashed, $Z = 3$; dotted, high- Z approximation (61). All the curves are built for $y_0 = 10^4$.

contributing particle trajectories are straighter, where-with typical partial momentum and energy transfers values are smaller, implying that so must be the cumulative $\lambda_m(\Theta)$. At moderately large Θ , in the semihard region [31], there are several relatively large-angle scatterings, so, the particle trajectories are the most crooked, where-with the energy loss is the largest. Finally, at $\Theta \rightarrow \infty$, when the trajectory is single-angle-shaped, $\lambda_m(\Theta) \rightarrow \lambda_m$, because even though the large energy loss in this single wide-angle scattering is large, in the straggling distribution it contributes beyond the region of typical losses.

V. HARD SCATTERING REGION. LARGE λ

Compared with the mild angle-energy loss correlation in the central region, studied in the previous section, in the hard scattering region the correlation must enhance, due to the increase of the relative contribution of single scattering events, each carrying a perfect correlation. But even there, multiple scattering effects need not disappear completely, because observation of an event with a large λ ascertains only that a single hard scattering on an atomic electron has occurred, whilst the number of soft elastic and inelastic scatterings may be arbitrary, and generally is large. Hence, even in the hard scattering region, effects of multiple scattering in the 2d distribution can be substantial, and thus need to be taken into account.

To be self-consistent, again, we should issue from double integral (26), which has to be formally evaluated in the corresponding limit. Actually, there are two possible ways of going to infinity in the Θ - λ plane, increasing one of the coordinates while holding the other of them fixed. It appears that those limits are noncommutable. Indeed, the limit $\Theta \rightarrow \infty$ implies typical $y \rightarrow 0$ in the integrand, whereas limit $\lambda \rightarrow \infty$ implies typical $u \rightarrow 0$.

But since Ω_{in} defined by Eq. (30) involves functions depending on the ratio y/u , the result must depend on the order, in which limits $y \rightarrow 0$ and $\lambda \rightarrow \infty$ are taken. The non-commutability of limits $\Theta \rightarrow \infty$ and $\lambda \rightarrow \infty$ is also evident from Fig. 3a, where at large λ there are two probability concentration regions separated by a void. Let us thus consider both limiting sequences by turn.

A. Fixed λ , large Θ

Let us begin with a simpler case $\Theta \rightarrow \infty$ at λ held fixed. The corresponding limiting form for F follows already from Eqs. (58) and (49):

$$F(Z, y_0, \Theta, \lambda) \underset{\Theta \rightarrow \infty}{\simeq} \frac{1}{\pi \Theta^4} \varphi_L(\lambda), \quad (62a)$$

or

$$f \underset{\theta \gg \chi_c}{\simeq} \frac{2mZ}{\pi p^2 \theta^4} \varphi_L[\lambda(Z, l, \epsilon)]. \quad (62b)$$

In particular, this proves that the maximum of F wrt λ , with the increase of Θ approaches λ_m for the pure Landau distribution [$\lambda_m(\Theta) \xrightarrow{\Theta \rightarrow \infty} \lambda_m$, see Fig. 10]. But since Eq. (58) was derived under condition (59), i.e., at limited λ , it remains questionable whether asymptotics (62) is valid at large λ .

In fact, this asymptotics can be rigorously proven to hold for any fixed λ . The proof begins with noting that limit $\Theta \rightarrow \infty$ at fixed λ in integral (26) implies $y \sim \Theta^{-2} \rightarrow 0$ at fixed u . The exponential $e^{\Omega_{el} + \Omega_{in}}$ may then be linearized in $\Omega_{el} = -\frac{y}{4} \ln \frac{y_0}{y}$ and $\Omega_{in}(y/4Z, u) - \Omega_{in}(0, u) \underset{y/4Zu \ll 1}{\simeq} \frac{y}{4Z}(2 + \ln u)$ [cf. Eq. (55)], but not in $\Omega_{in}(0, u) = u \ln u$:

$$F(Z, y_0, \Theta, \lambda) = \frac{1}{2\pi i} \int_{-i\infty}^{i\infty} du e^{\lambda u + u \ln u} \times \frac{1}{4\pi} \int_0^{y_{\max}} dy J_0(\sqrt{y}\Theta) \left[-\frac{y}{4} \ln \frac{y_0}{y} + \frac{y}{4Z}(2 + \ln u) \right]. \quad (63)$$

Employing here identity

$$\int_0^\infty dy y J_0(\sqrt{y}\Theta) = 0 \quad (\Theta > 0) \quad (64)$$

along with relation (49), from (63) we infer asymptotic law (62a) for any fixed λ . To be precise, it holds if $\Theta^2 \gg 1$, and at the same time $\Theta^{-2} \sim y \ll Zu \sim Z/\lambda$, i.e.,

$$\Theta^2 \gg \lambda/Z, 1. \quad (65)$$

The factorization in this limit of the distribution function into Rutherford asymptotics θ^{-4} times Landau distribution depending on λ physically corresponds to the dominance of events involving one hard scattering on an atomic nucleus (while hard scattering on an atomic electron is excluded by requiring the energy transfer to be

limited), preceded and followed by statistically independent soft scatterings, whose energy straggling is described by the Landau distribution.

It should be emphasized, however, that factorization (62) is inequivalent to absence of correlation expressed by Eq. (52). The latter would imply

$$F \approx \frac{Z}{Z+1} \varphi_L(\lambda) \frac{\chi_c^4}{\pi \theta^4} = \frac{Z+1}{Z} \frac{1}{\pi \Theta^4} \varphi_L(\lambda), \quad (66)$$

with an extra factor $\frac{Z+1}{Z}$ including hard scattering on atomic electrons, already mentioned in Sec. III C. Hence, the correlation in this region does not vanish, but the only reason is that hard scattering on electrons is excluded by presuming λ to be limited.

B. Large λ , fixed Θ

In the limit $\lambda \rightarrow \infty$, typical u in the Fourier integral tend to zero. That does not allow expanding the exponent in powers of u yet, because of its non-analyticity at $u = 0$. But since the difference $\Omega_{in}(y/4Z, u) - \Omega_{in}(y/4Z, 0)$ in this limit is “almost uniformly” small (see Fig. 1),⁷ the exponential may be expanded in this difference. Thereafter, double partial integration over u with the aid of identity (33) yields

$$\begin{aligned} F(Z, y_0, \Theta, \lambda) &\underset{\lambda \rightarrow \infty}{\simeq} \frac{1}{4\pi\lambda^2} \\ &\times \int_0^{y_{\max}} dy J_0(\sqrt{y}\Theta) e^{\Omega_{el}(y_0, y) + \Omega_{in}(y/4Z, 0)} \\ &\times \frac{1}{2\pi i} \int_{-i\infty}^{i\infty} du e^{\lambda u} \frac{\partial^2}{\partial u^2} \left[\Omega_{in}\left(\frac{y}{4Z}, u\right) - \Omega_{in}\left(\frac{y}{4Z}, 0\right) \right] \\ &= \frac{1}{4\pi\lambda^2} \int_0^{y_{\max}} dy J_0(\sqrt{y}\Theta) e^{\Omega_{el}(y_0, y) + \Omega_{in}(y/4Z, 0)} \\ &\quad \times \frac{1}{2\pi i} \int_{-i\infty}^{i\infty} \frac{du}{u} e^{\lambda u - y/4Z u}. \quad (68) \end{aligned}$$

The latter u -integral is a well-known representation for zero-order Bessel function [35]:

$$\frac{1}{2\pi i} \int_{-i\infty}^{i\infty} \frac{du}{u} e^{\lambda u - \frac{y}{4Z} u} = J_0(\sqrt{y}\Psi),$$

where

$$\Psi(\lambda) = \sqrt{\lambda/Z}. \quad (69)$$

⁷ Strictly speaking, derivative

$$\left. \frac{\partial \Omega_{in}}{\partial u} \right|_{u=0} = \ln Y + 1 + \gamma_E \quad (67)$$

diverges at small and at large Y , but only logarithmically. This can be easily compensated by a sufficient smallness of u .

Combining logarithms in the exponent $\Omega_{el}(y_0, y) + \Omega_{in}(y/4Z, 0)$ as in Eq. (43), and accordingly changing the integration variable from y to η , we are led to the asymptotic expression

$$F(Z, y_0, \Theta, \lambda) \underset{\lambda \rightarrow \infty}{\simeq} \frac{Z}{(Z+1)\lambda^2} \beta_M \left(\frac{4\chi_c^2}{\chi_{at}^2}, \frac{\theta}{\chi_c}, \sqrt{\frac{\lambda}{Z+1}} \right), \quad (70)$$

with

$$\beta_M(\eta_0, \Theta, \Psi) = \frac{1}{4\pi} \int_0^{\eta_{\max}} d\eta J_0(\sqrt{\eta}\Theta) J_0(\sqrt{\eta}\Psi) e^{-\frac{\eta}{4} \ln \frac{\eta_0}{\eta}} \quad (71a)$$

$$= \frac{1}{2\pi} \int d\phi_{\Theta\Psi} \varphi_M(\eta_0, |\Theta - \Psi|) \quad (71b)$$

$$= \frac{2}{\pi} \int_{|\Theta-\Psi|}^{\Theta+\Psi} \frac{dz z \varphi_M(\eta_0, z)}{\sqrt{[(\Theta + \Psi)^2 - z^2][z^2 - (\Theta - \Psi)^2]}}. \quad (71c)$$

Function (71), symmetrically depending on variables Θ and Ψ , is normalized by

$$2\pi \int_0^\infty d\Theta \Theta \beta_M(\eta_0, \Theta, \Psi) = 1.$$

It arises also in other multiple Coulomb scattering problems [15, 32].

Evidently, distribution (70), (71b) describes the probability of a two-stage process: a single hard scattering on an atomic electron through an angle Ψ corresponding to the energy loss λ , and subsequent multiple elastic and inelastic scattering from Ψ to angle Θ with a prescribed modulus Θ . The factor λ^{-2} in (70) is nothing but the high- λ asymptotics of $\varphi_L(\lambda)$ [cf. Eq. (39)]. Compared to (58), however, the dependence on λ in the factorized structure (70) at large λ enters not to the thickness parameter y_0 , but to the angular variable $\Psi(\lambda)$ on equal footing with Θ . The accuracy of this approximation is illustrated in Figs. 3b,c, 4b,c by dot-dashed curves, showing that it works well for $\lambda \gtrsim 20$.

We are primarily interested in behavior of β_M at large Ψ . There it admits further simplifications. In particular, if $|\Theta - \Psi|$ is substantially smaller than Ψ , one can neglect in the denominator of (71c) z^2 compared with $(\Theta + \Psi)^2$, but not compared with $(\Theta - \Psi)^2$. That leads to an approximation

$$\beta_M(\eta_0, \Theta, \Psi) \simeq \frac{1}{\pi(\Theta + \Psi)} \varphi_{Mx}(\eta_0, \Theta - \Psi), \quad (72)$$

where

$$\varphi_{Mx}(\eta_0, \Theta_x) = \frac{1}{\pi} \int_0^{\sqrt{\eta_{\max}}} dx \cos(\Theta_x x) e^{-\frac{x^2}{4} \ln \frac{\eta_0}{x^2}} \quad (73)$$

is the projection of the Molière distribution onto one Cartesian component of Θ [31] [the averaging over a circle in Eq. (71b) is replaced by integration over the tangential line to it in a point $\Psi(1 - \Theta/\Psi)$ nearest to the

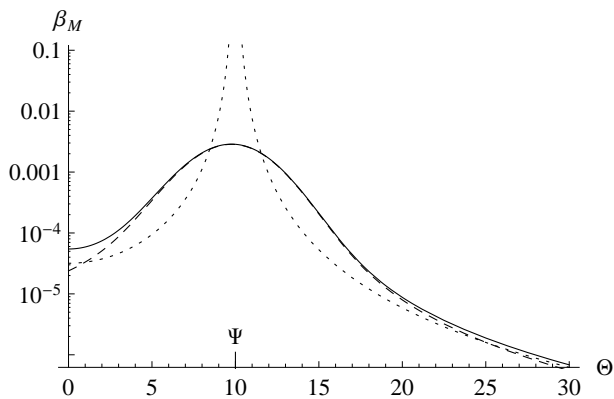


FIG. 11: Coulomb rescattering probability distribution (71a) for $\eta_0 = 10^4$, $\Psi = 10$ ($\lambda = 100Z^2$). Dashed curve, large- Ψ approximation (72), (73). Dotted, double hard scattering approximation (74).

origin]. This approximation is confronted with the exact result (70), (71a) in Fig. 11. Its accuracy is the highest near the top of the distribution, but degrades away from it, where $(\Theta - \Psi)^2$ is no longer small compared with $(\Theta + \Psi)^2$.

If Ψ and Θ are about equally large, the argument of φ_M in the integrand of (71b) or (71c) is everywhere large, as well. Then, pure Rutherford asymptotics (49) applies, wherewith the integral simply evaluates to give

$$\beta_M(y_0, \Theta, \Psi) \underset{\Theta, \Psi, |\Theta - \Psi| \gg 1}{\approx} \frac{\Theta^2 + \Psi^2}{\pi |\Theta^2 - \Psi^2|^3}. \quad (74)$$

One implication thereof is that at Θ held fixed and Ψ sent to infinity, function β_M decreases as $\beta_M \underset{\Psi \rightarrow \infty}{\sim} \Psi^{-4} \sim \lambda^{-2}$, which, according to Eq. (70), corresponds to the large- λ asymptotic behavior for F :

$$F \underset{\lambda \rightarrow \infty}{\sim} \lambda^{-4}. \quad (75)$$

Besides that, Eq. (74) predicts a Rutherford-like asymptotics at $\Theta \rightarrow \infty$. But insertion of (74) to Eq. (70) yields

$$F \underset{\theta \gg \chi_c}{\approx} \frac{Z}{(Z+1)\pi\lambda^2} \left(\frac{\chi_c}{\theta}\right)^4 = \frac{Z+1}{Z\pi\lambda^2\Theta^4}, \quad (76)$$

which due to the $\frac{Z+1}{Z}$ factor matches with (66), corresponding to the absence of correlation, and somewhat differing from the correct asymptotics (62). Therefore, at sufficiently large θ/χ_c approximation (70) breaks down. That is also confirmed by Figs. 3b, 4b.

VI. PARTIAL MEAN VALUES

In the previous section, studying the correlation in the 2-variable distribution function, we had seen that the

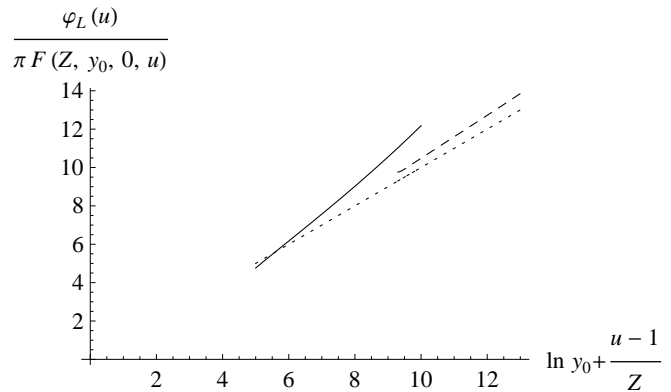


FIG. 12: Inverse of the angular distribution function at zero deflection angle, serving as a counterpart of the mean square deflection angle. Solid curve, $y_0 = 10^3$, $Z = 1$. Dashed curve, $y_0 = 10^3$, $Z = 3$. Dot-dashed, $y_0 = 10^6$, $Z = 1$. Dotted line, LLA (78).

correlation between Θ and λ strengthens at large values of those variables. But the quadratic decrease of the probability density with λ can hamper experimental observation of the correlation effects in this region. In view of that, advantageous may be experimental setups directly measuring net characteristics of the distribution, such as partial mean values and widths. Due to the momentum or energy weighting factors involved therein, the relative contribution of the hard component to them may enhance. To accomplish our study, we will investigate manifestations of the correlation directly for such net quantities.

A. Energy loss dependence of angular dispersion

The shape of the angular distribution at fixed λ , at least when λ is moderate, is symmetric and bell-like, so, the measure of its width could be the mean square deflection angle. But Rutherford asymptotics of the distribution at large Θ in principle leads to a logarithmic divergence of $\langle \Theta^2 \rangle$ for any λ . As a counterpart of $\langle \Theta^2 \rangle$, which is finite and simply related with the distribution function, one can merely take the inverse of the distribution function in the origin [cf. Eq. (50)]:

$$\frac{\varphi_L(\lambda)}{\pi F(Z, y_0, 0, \lambda)} \approx \frac{1}{\pi \varphi_M(y_0 K, 0)}. \quad (77)$$

If, moreover, we employ here the LLA approximation (50), it becomes

$$\frac{\varphi_L(\lambda)}{\pi F(Z, y_0, 0, \lambda)} \approx \ln y_0 K = \ln y_0 + \frac{\lambda - 1}{Z}. \quad (78)$$

Approximation (78), slowly improving with the increase of y_0 , rises linearly with λ , provided the λ -dependent contribution is relatively small, satisfying condition (59). This linear law may be thought of as a sum of soft ($\ln y_0$)

and hard ($\frac{\lambda-1}{Z}$) contributions. At larger λ , the distribution shape becomes non-Gaussian and (77) can no longer serve as a measure of the mean squared deflection angle. As Fig. 13 indicates, the exact ratio (77) rises with λ linearly, as well, but this slope appreciably differs from (78). Instead, the latter becomes strongly influenced by location $\Theta \approx \Psi = \sqrt{\lambda/Z}$ of the slice of the spur. Squaring this, we see that the effective $\langle \Theta^2 \rangle$ continues growing linearly with λ/Z .

B. Angular dependence of the mean energy loss

In what concerns the energy straggling distribution, which is highly asymmetric, its principal net characteristic is the mean energy loss. Historically, measurements of this quantity at fixed angles for incident ions, by means of magnetic spectrometry, were the first to give experimental evidence of the positive angle-energy loss correlation. Magnetic spectrometry is applicable for relativistic electrons, too. Another option is to use a sufficiently large solid-state detector, registering events up to very high λ , summation over which can give the mean ionization energy loss at a fixed deflection angle.

Since energy loss is linearly related to the reduced variable λ [see Eq. (25)], their mean values are linearly related, as well:

$$\begin{aligned} \bar{\epsilon}(\theta) &= \frac{\int_0^\infty d\epsilon \epsilon f(\theta, \epsilon)}{\int_0^\infty d\epsilon f(\theta, \epsilon)} \\ &= \frac{p^2 Z \bar{\chi}_c^2}{2m} \left[\ln \frac{p^2 \gamma^2 Z \bar{\chi}_c^2}{I_\delta^2} - \gamma_E + \gamma^{-2} + \bar{\lambda}(\Theta) \right], \end{aligned} \quad (79)$$

with⁸

$$\bar{\lambda}(\Theta) = \frac{\int_{-\infty}^\infty d\lambda \lambda F(Z, y_0, \Theta, \lambda)}{\int_{-\infty}^\infty d\lambda F(Z, y_0, \Theta, \lambda)}. \quad (80)$$

Granted that function F decreases at large λ faster than φ_L [see Eqs. (75), (39)], the integral in the numerator of (80) converges.

Whereas for Landau distribution, exhibiting asymptotics (39), integral $\int_{-\infty}^\infty d\lambda \lambda \varphi_L(\lambda)$ logarithmically diverges at the upper limit (implying that to evaluate the physical mean energy loss, one needs to take into account its limitation by the initial electron energy E), a similar integral $\int_{-\infty}^\infty d\lambda \lambda F(Z, y_0, \Theta, \lambda)$ at any fixed Θ converges, because according to Eq. (75), F decreases more rapidly than φ_L . But asymptotics (75) only sets in beyond the ‘‘spur’’, i.e., greater than

$$\lambda_{\max}(\Theta) \sim Z\Theta^2 = (Z+1)\theta^2/\chi_c^2 \quad (81)$$

⁸ By virtue of the rapid convergence of integrals in (80), we have replaced its actual lower integration limit $-\ln \frac{p^2 \gamma^2 Z \bar{\chi}_c^2}{I_\delta^2} + \gamma_E - \gamma^{-2}$ in by $-\infty$.

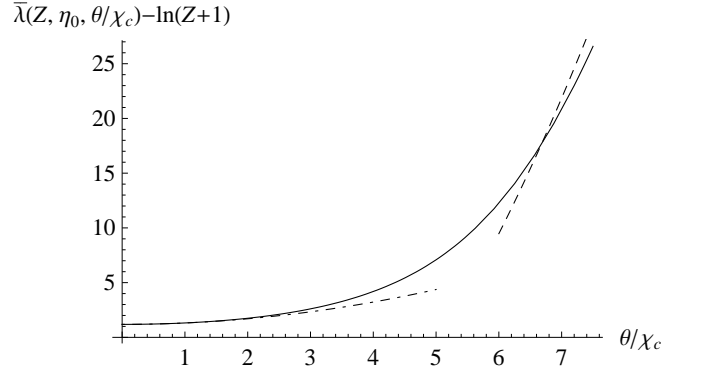


FIG. 13: Solid curve, dependence of the mean energy loss defined by Eq. (83a) on the scattering angle, at $\eta_0 = 10^4$. Dot-dashed curve, approximation (85). Dashed curve, approximation (88).

[see Eqs. (34), (69)]. So, in effect, this spur imposes a lower cutoff $\lambda_{\max}(\Theta)$ than that imposed by E .

Our task then is to evaluate ratio (80), which can be done best by substituting there the integral representation (26) for F . With the use of identity (31) and its derivative

$$\int_{-\infty}^\infty d\lambda \lambda \frac{1}{2\pi i} \int_{-i\infty}^{i\infty} du e^{\lambda u + \Omega_{in}(Y, u)} = - \frac{\partial}{\partial u} e^{\Omega_{in}(Y, u)} \Big|_{u=0},$$

we recast (80) as

$$\begin{aligned} \bar{\lambda}(\Theta) &= - \left[\int_0^{y_{\max}} dy J_0(\sqrt{y}\Theta) e^{-\frac{3}{4} \ln \frac{y_0}{y}} \right]^{-1} \\ &\quad \times \int_0^{y_{\max}} dy J_0(\sqrt{y}\Theta) e^{\Omega_{el}(y_0, y) + \Omega_{in}(y/4Z, 0)} \\ &\quad \times \frac{\partial}{\partial u} \Omega_{in}(y/4Z, u) \Big|_{u=0}. \end{aligned} \quad (82)$$

Substituting $\frac{\partial}{\partial u} \Omega_{in} \Big|_{u=0}$ from Eq. (67), next we transform (82) to

$$\begin{aligned} \bar{\lambda}(Z, \eta_0, \theta/\chi_c) &= \frac{\int_0^{\eta_{\max}} d\eta J_0(\sqrt{\eta}\theta/\chi_c) e^{-\frac{3}{4} \ln \frac{\eta_0}{\eta}} \ln \frac{1}{\eta}}{\int_0^{\eta_{\max}} d\eta J_0(\sqrt{\eta}\theta/\chi_c) e^{-\frac{3}{4} \ln \frac{\eta_0}{\eta}}} \\ &\quad + \ln 4(Z+1) - 1 - \gamma_E, \end{aligned} \quad (83a)$$

where

$$\eta_0 = \frac{4\chi_c^2}{\chi_{at}^2}.$$

The integral in the denominator is recognized to equal $4\pi\varphi_M(\eta_0, \theta/\chi_c)$. Representation (79), (83a) can as well be derived directly from the generic solution (3), (4) of the transport equation (see Appendix B).

Examination of the numerator of (83a) now shows that it can be expressed via φ_M , as well. To this end, it is

expedient first to integrate in the numerator by parts:

$$\bar{\lambda}(Z, \eta_0, \theta/\chi_c) = -\frac{\int_0^{\eta_{\max}} d\eta J_0(\sqrt{\eta}\theta/\chi_c) \frac{\partial}{\partial \eta} e^{-\frac{\eta}{4} \ln \frac{\eta_0}{\eta}}}{\pi \varphi_M(\eta_0, \theta/\chi_c)} - \ln \frac{\eta_0}{4(Z+1)} - \gamma_E, \quad (83b)$$

where

$$\ln \frac{\eta_0}{4(Z+1)} + \gamma_E = \frac{Z+1}{Z} \left(\ln \frac{Z \bar{\chi}_c^2}{\chi_{at}^2} + \gamma_E \right).$$

Thereupon, integrating in (83b) by parts, employing identity

$$\frac{\partial}{\partial \eta} J_0(\sqrt{\eta}\theta/\chi_c) = -\frac{1}{2} \int_0^{\theta/\chi_c} d\Psi \Psi J_0(\sqrt{\eta}\Psi)$$

(an integral form of the Bessel equation $\frac{d}{d\xi} \xi \frac{d}{d\xi} J_0(\xi) = -\xi J_0(\xi)$, $J_0'(0) = 0$), and interchanging the order of η - and Ψ -integrations, one can express the angular dependence of the mean energy loss completely through the Molière function φ_M :

$$\bar{\lambda}(Z, \eta_0, \theta/\chi_c) = \frac{2 \int_{\theta/\chi_c}^{\infty} d\Psi \Psi \varphi_M(\eta_0, \Psi)}{\varphi_M(\eta_0, \theta/\chi_c)} - \ln \frac{\eta_0}{4(Z+1)} - \gamma_E. \quad (83c)$$

In contrast to the representation (B1), it is explicitly independent of the underlying single-scattering differential cross-section, except the dependence on χ'_{at} entering η_0 . Note, too, that for a given η_0 , the θ -dependent part of $\bar{\lambda}$ is independent of Z . That property may be beneficial for practice.

In the LLA (50), the ratio represented by the first term in Eq. (83c) equals $\ln \eta_0$, exactly canceling the similar η_0 -dependence in the second term, wherewith

$$\bar{\lambda}(Z, \eta_0, \theta/\chi_c) \approx \ln 4(Z+1) - \gamma_E.$$

The value obtained in this approximation is then θ -independent, whereas its logarithmic Z dependence owes merely to the existence of the effective Z -dependent cut-off (81). In reality, though, as is illustrated in Fig. 13, function $\bar{\lambda}(Z, \eta_0, \theta/\chi_c)$ monotonously increases with θ . We will show below that its θ dependence is quadratic both at $\theta/\chi_c \rightarrow 0$ and $\theta/\chi_c \rightarrow \infty$, but with different coefficients.

1. Small θ/χ_c

The minimal value of the monotonously rising function $\bar{\lambda}(Z, \eta_0, \theta/\chi_c)$, achieved at $\theta = 0$, is

$$\bar{\lambda}(Z, \eta_0, 0) = \frac{1}{\pi \varphi_M(\eta_0, 0)} - \ln \frac{\eta_0}{4(Z+1)} - \gamma_E. \quad (84)$$

This value is positive, and thence greater than MPEL [cf. Eq. (40)], which is natural in view of high skewness of

$\bar{\lambda}(Z, \eta_0, 0) - \ln(Z+1)$

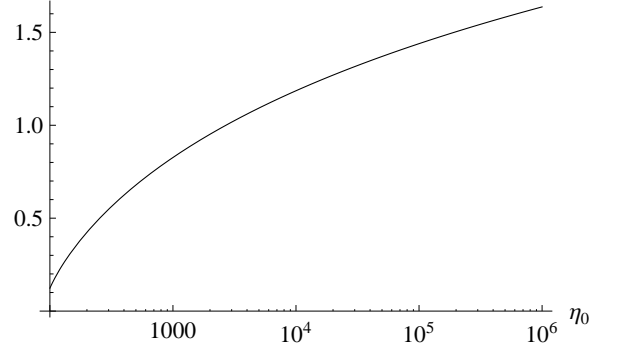


FIG. 14: Target thickness dependence of the mean energy loss in the forward direction [Eq. (84)].

the λ -distribution. It also depends on η_0 , but slower than logarithmically (see Fig. 14). The $\mathcal{O}(\theta^2/\chi_c^2)$ correction to (84) has the form

$$\bar{\lambda}(Z, \eta_0, \theta/\chi_c) \underset{\theta/\chi_c \rightarrow 0}{\simeq} \bar{\lambda}(Z, \eta_0, 0) + \Lambda_2(\eta_0) \frac{\theta^2}{\chi_c^2}, \quad (85)$$

with

$$\begin{aligned} \Lambda_2(\eta_0) &= \chi_c^2 \left. \frac{\partial \bar{\lambda}}{\partial \theta^2} \right|_{\theta=0} = \frac{\partial}{\partial \ln \eta_0} \bar{\lambda}(Z, \eta_0, 0) \\ &= \frac{\partial}{\partial \ln \eta_0} \frac{1}{\pi \varphi_M(\eta_0, 0)} - 1. \end{aligned} \quad (86)$$

In the LLA [see Eq. (50)], the difference in the rhs of (86) would equal zero, similarly to the conclusion reached in [33] for ions, but in reality, as is demonstrated by Fig. 15, it is sizable enough.

2. Large θ/χ_c

The quadratic θ -dependence of $\bar{\lambda}(Z, \eta_0, \theta/\chi_c)$, as a whole, continues in the hard region, but the coefficient at it changes. Employing the known expansion [31]

$$\pi \varphi_M(\eta_0, \theta/\chi_c) \underset{\theta/\chi_c \rightarrow \infty}{\simeq} \frac{\chi_c^4}{\theta^4} + \frac{4\chi_c^6}{\theta^6} \left(\ln \frac{\theta^2}{\chi_{at}^2} + 2\gamma_E - 3 \right) \quad (87)$$

(including the correction to the Rutherford asymptotics of φ_M at high θ/χ_c), integrating it as

$$\begin{aligned} &2\pi \int_{\theta/\chi_c}^{\infty} d\Psi \Psi \varphi_M(\eta_0, \Psi) \\ &\underset{\theta/\chi_c \rightarrow \infty}{\simeq} \frac{\chi_c^2}{\theta^2} + \frac{4\chi_c^4}{\theta^4} \left(\frac{1}{2} \ln \frac{\theta^2}{\chi_{at}^2} + \gamma_E - \frac{5}{4} \right), \end{aligned}$$

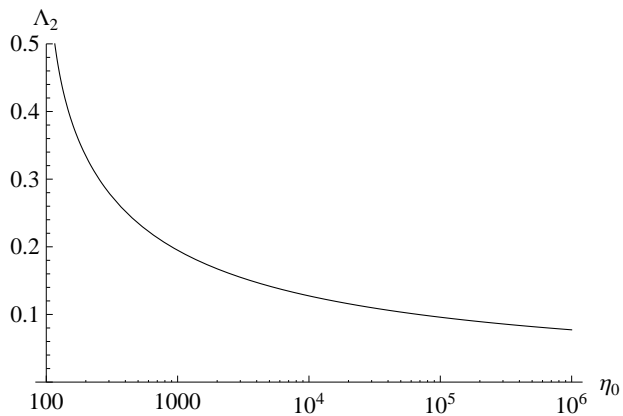


FIG. 15: Target thickness dependence of the coefficient at the quadratic term in the $\bar{\lambda}$ dependence on θ at small θ/χ_c [Eqs. (85), (86)].

and inserting to representation (83c), we get

$$\bar{\lambda}(Z, \eta_0, \theta/\chi_c) \underset{\theta/\chi_c \rightarrow \infty}{\simeq} \frac{\theta^2}{\chi_c^2} \frac{1 + \frac{4\chi_c^2}{\theta^2} \left(\frac{1}{2} \ln \frac{\theta^2}{\chi_{at}^2} + \gamma_E - \frac{5}{4} \right)}{1 + \frac{4\chi_c^2}{\theta^2} \left(\ln \frac{\theta^2}{\chi_{at}^2} + 2\gamma_E - 3 \right)} - \ln \frac{\eta_0}{4(Z+1)} - \gamma_E$$

$$\underset{\theta/\chi_c \rightarrow \infty}{\simeq} \frac{\theta^2}{\chi_c^2} - 2 \ln \frac{\theta^2}{\chi_{at}^2} - 5\gamma_E + 7 - \ln \frac{\eta_0}{4(Z+1)}. \quad (88)$$

This asymptote is plotted in Fig. 13 by a dashed curve.

Physically, the leading-order term θ^2/χ_c^2 in (88), of course, corresponds to a single hard scattering on an atomic electron, but as compared with relationship (81) obtained in the previous section, the proportionality coefficient in this term does not involve a factor of $Z+1$. That is explained by noting that albeit scattering on an electron through a large angle θ does give a contribution to λ equal $(Z+1)\theta^2/\chi_c^2$ [cf. Eqs. (70), (81)], the probability of scattering to angle Θ on an electron, and not on a nucleus (which does not change λ), is $1/(Z+1)$. Those Z -dependent factors cancel in the mean λ value.

Less trivial is the correction term in (88), logarithmically depending on θ . Structurally, it corresponds to a double hard scattering [31] – on an electron and on an atomic nucleus, but it enters with a negative coefficient. That can be made plausible as follows. In an event containing one hard inelastic scattering act, there is a contribution to the aggregate deflection angle from elastic scattering, which adds (incoherently) to the deflection angle squared. Hence, the scattering angle squared acquired only in the hard collision with an atomic electron is smaller than that observed.

VII. SUMMARY

The unification of Molière and Landau theories presented herein reveals a pronounced correlation between

the deflection angle and ionization energy loss for ultra-relativistic electrons or positrons traversing amorphous matter. The correlation arises at the single-scattering level, but sustains multiple Coulomb scattering, as well, due to the anomalous character of the latter. The target thickness dependence of the correlation effect is thus mild. As for its Z -dependence, the angular distribution in the central region (moderate Θ and λ) primarily depends on the ratio of the straggling variable λ to Z (see Fig. 12). Therefore, even for high- Z target materials, in principle, there are manifestations of the correlation at proportionally high λ , but they are obscured by a falloff of the event rate with the increase of λ . An advantageous observable at high Z is the mean energy loss as a function of the deflection angle, whose variable part, representing the correlation effect, is independent of Z (see Sec. VIB).

It is worth emphasizing that the hard incoherent scattering mechanism responsible for the angle-energy loss correlation for fast electrons is different from those at work for slow ions, mentioned in the Introduction. Whereas interaction of a non-relativistic ion with an atom is amenable to semiclassical treatment, when each impact parameter corresponds to a well-defined scattering angle, as well as energy loss, for relativistic electrons the angle and the energy loss are distributed statistically. In spite of that, their mutual correlation is not small, because it is dominated by hard electron-electron scattering, in which the deflection angle and energy transfer are interrelated kinematically, regardless of the impact parameter wrt the atomic nucleus. Moreover, it is precisely this contribution which survives under multiple scattering conditions.

At the same time, the hard incoherent scattering correlation exhibits certain formal similarities with mechanisms previously discussed for heavy ions. Viz., in the central, moderate scattering angle and energy loss region, the angular distribution broadens with the increase of the energy loss straggling variable, as if the effective path length of the electron in the target acquired a dependence on the energy loss (see Sec. IV). That should be distinguished from the genuine extension of the particle path length due to the trajectory curvature (“detour”), which is too small at high energy. There is also a similarity with the impact-parameter-mediated correlation, with the proviso that the role of the impact parameter is played by the Fourier-reciprocal of the scattering angle on the probability level (see Sec. II).

The mentioned similarities hold only in the central region. The most prominent feature in the correlated distribution function, though, is a spur in the large deflection angle and energy loss region. It corresponds to a quasifree ee scattering, but in contrast to the underlying delta-function (8), is significantly smeared by multiple scattering effects (see Sec. V).

Experimental verification of the predicted correlation should be feasible with silicon (lowest- Z semiconductor) targets, by observing $\sim Z^{-1} \approx 10\%$ differences between

angular distributions measured at different values of ionization energy loss (see Fig. 6). Stronger correlation effects ($\sim Z^{-1} \approx 20\%$, see Fig. 5) may become measurable in future with the advent of organic semiconductors, developed nowadays for flexible electronics [34].

Acknowledgements

This work was supported in part by the National Academy of Sciences of Ukraine (projects 0118U100327 and 0118U006496) and the Ministry of Education and Science of Ukraine (project 0118U002031).

Appendix A: Evaluation of integral (20)

Evaluation of integral (20) with the NLL accuracy can be performed, e. g., by decomposing the Bessel function into power series, $J_0(b\chi) = \sum_{n=0}^{\infty} (n!)^{-2} (-b^2\chi^2/4)^n$, and integrating termwise:

$$\begin{aligned} & \int_{\chi_1}^{\infty} \frac{d\chi}{\chi^3} \left[1 - J_0(b\chi)e^{-s\chi^2} \right] \\ &= \frac{1}{2\chi_1^2} - \sum_{n=0}^{\infty} \frac{1}{(n!)^2} \left(-\frac{b^2}{4} \right)^n \int_{\chi_1}^{\infty} d\chi \chi^{-3+2n} e^{-s\chi^2}. \quad (\text{A1}) \end{aligned}$$

In the obtained series, terms with $n \geq 2$ have integrands non-singular at $\chi \rightarrow 0$, so, in the limit $\chi_1 \rightarrow 0$ within the present accuracy it is legitimate just to let there $\chi_1 = 0$. Terms with $n = 0$ and $n = 1$ have singular integrands, but they can be evaluated exactly:

$$\begin{aligned} & \int_{\chi_1}^{\infty} \frac{d\chi}{\chi^3} \left[1 - J_0(b\chi)e^{-s\chi^2} \right] \\ &= \frac{1}{2\chi_1^2} - \int_{\chi_1}^{\infty} \frac{d\chi}{\chi^3} e^{-s\chi^2} + \frac{b^2}{4} \int_{\chi_1}^{\infty} \frac{d\chi}{\chi} e^{-s\chi^2} \\ &\quad - \sum_{n=2}^{\infty} \frac{1}{(n!)^2} \left(-\frac{b^2}{4} \right)^n \int_0^{\infty} d\chi \chi^{-3+2n} e^{-s\chi^2} \\ &\equiv \frac{1}{2\chi_1^2} \left(1 - e^{-s\chi_1^2} \right) + \frac{1}{2} \left(s + \frac{b^2}{4} \right) E_1(s\chi_1^2) \\ &\quad - \frac{s}{2} \sum_{n=2}^{\infty} \frac{1}{(n-1)nn!} \left(-\frac{b^2}{4s} \right)^n, \quad (\text{A2}) \end{aligned}$$

where $E_1(z) = \int_z^{\infty} \frac{d\xi}{\xi} e^{-\xi}$ is the exponential integral function [35]. At small $s\chi_1^2$, the terms in the first line may be approximated by

$$\frac{1}{2\chi_1^2} \left(1 - e^{-s\chi_1^2} \right) \underset{s\chi_1^2 \ll 1}{\approx} \frac{s}{2}, \quad (\text{A3})$$

$$E_1(s\chi_1^2) \underset{s\chi_1^2 \ll 1}{\approx} \ln \frac{1}{s\chi_1^2} - \gamma_E. \quad (\text{A4})$$

The series in the last line of (A2), after decomposing the fraction into simpler ones as

$$\frac{1}{(n-1)nn!} = \frac{1}{(n-1)(n-1)!} - \frac{1}{nn!} - \frac{1}{n!},$$

evaluates in a closed form:

$$\sum_{n=2}^{\infty} \frac{(-z)^n}{(n-1)nn!} = 1 - e^{-z} - 2z + (1+z) \text{Ein}(z) \geq 0, \quad (\text{A5})$$

involving the complementary exponential integral function [35]

$$\begin{aligned} \text{Ein}(z) &= - \sum_{n=1}^{\infty} \frac{(-z)^n}{nn!} = \int_0^z \frac{1 - e^{-\xi}}{\xi} d\xi \\ &= \gamma_E + \ln z + E_1(z). \quad (\text{A6}) \end{aligned}$$

Inserting (A3)–(A5) in Eq. (A2), we are led to Eq. (22).

In limit $s \rightarrow 0$, (22) correctly goes over to (21), whereas in limit $b \rightarrow 0$, to the readily checkable expression

$$\begin{aligned} & \int_{\chi_1}^{\infty} \frac{d\chi}{\chi^3} \left(1 - e^{-s\chi^2} \right) \\ &= s \lim_{b \rightarrow 0} \left[\ln \frac{2}{b\chi_1} - \frac{1}{2} E_1 \left(\frac{b^2}{4s} \right) + \frac{1}{2} - \gamma_E \right] \\ &= \frac{s}{2} \left(\ln \frac{1}{s\chi_1^2} + 1 - \gamma_E \right). \quad (\text{A7}) \end{aligned}$$

Appendix B: Correspondence of Eq. (83) with [15]

In application to angular dependence of the mean energy loss, it is instructive to establish correspondence of our expressions (79), (83) for this quantity with representation

$$\bar{\epsilon}(l, \theta) = \frac{n_a l}{f(l, \theta)} \iint d\sigma_{in}(\chi, \Delta\epsilon) \Delta\epsilon f(l, |\theta - \chi|) \quad (\text{B1})$$

derived in [15]. Eq. (B1) explicitly involves the single-scattering differential cross-section, but under the conditions of multiple scattering, it is likely that little should depend on its detail.

To prove that, we return to the generic solution (3), (4) of the transport equation in terms of single-scattering cross-sections, and insert it to the definition (79) of the mean energy loss at a fixed θ :

$$\begin{aligned} \bar{\epsilon}(l, \theta) &= \frac{\int_0^{\infty} d\epsilon \epsilon f(l, \theta, \epsilon)}{f(l, \theta)} \\ &= \frac{p^2}{2m} \frac{l}{2\pi f(l, \theta)} \int_0^{\infty} db b J_0(b\theta) e^{-l\kappa(b,0)} \left. \frac{\partial \kappa}{\partial s} \right|_{s=0} \\ &= \frac{n_a l}{2\pi f(l, \theta)} \int_0^{\infty} db b J_0(b\theta) e^{-l\kappa(b,0)} \\ &\quad \times \iint d\sigma_{in}(\chi, \Delta\epsilon) \Delta\epsilon J_0(b\chi). \quad (\text{B2}) \end{aligned}$$

If we interchange in (B2) the order of integrations,

$$\bar{\epsilon}(l, \theta) = \frac{n_a l}{f(l, \theta)} \iint d\sigma_{in}(\chi, \Delta\epsilon) \Delta\epsilon \int \frac{d^2b}{(2\pi)^2} e^{ib \cdot (\theta - \chi) - l\kappa(b, 0)}, \quad (\text{B3})$$

it is brought to form (B1).

If instead we adopt the multiple scattering approximation, similar to that of Sec. II, integral (B2) breaks in two:

$$\begin{aligned} & n_a l \iint d\sigma_{in}(\chi, \Delta\epsilon) \Delta\epsilon J_0(b\chi) \\ &= n_a l \iint_{\chi < \chi_1} d\sigma_{in}(\chi, \Delta\epsilon) \Delta\epsilon + \frac{p^2}{2m} 2Z\bar{\chi}_c^2 \int_{\chi_1}^{\infty} \frac{d\chi}{\chi} J_0(b\chi), \end{aligned} \quad (\text{B4})$$

where in the first term in the rhs we have let $J_0(b\chi) \rightarrow J_0(0) = 1$, while in the second one, employed Rutherford asymptotics (8). If we now utilize Eq. (15) along with identity

$$\int_{\chi_1}^{\infty} \frac{d\chi}{\chi} J_0(b\chi) \underset{b\chi_1 \rightarrow \infty}{\simeq} \ln \frac{2}{b\chi_1} - \gamma_E,$$

the delimiting parameter χ_1 cancels out, and we are left

with

$$\begin{aligned} & n_a l \iint d\sigma_{in}(\chi, \Delta\epsilon) \Delta\epsilon J_0(b\chi) \\ &= \frac{Z}{m} p^2 \bar{\chi}_c^2 \left(\ln \frac{2p\gamma}{bI_\delta} - \frac{v^2}{2c^2} - \gamma_E \right). \end{aligned} \quad (\text{B5})$$

Insertion thereof to Eq. (B2),

$$\begin{aligned} \bar{\epsilon}(l, \theta) &= \frac{p^2 Z \bar{\chi}_c^2}{2m f(l, \theta)} \frac{1}{2\pi} \int_0^\infty db b J_0(b\theta) e^{-l\kappa(b, 0)} \\ &\quad \times \left(2 \ln \frac{2p\gamma}{bI_\delta} - \frac{v^2}{c^2} - 2\gamma_E \right), \end{aligned} \quad (\text{B6})$$

leads back to Eqs. (79), (83a). According to (83c), this is expressible completely through φ_M , without the need to know the differential inelastic cross-section $d\sigma_{el}$.

Therefore, in the multiple scattering regime the entire sensitivity to the single-scattering cross-section reduces to I_δ . Furthermore, in the ultrarelativistic limit, due to the density effect, it reduces to the mean electron density, which is determined by Z .

-
- [1] G. Molière, Z. Naturforsch. **3a**, 78 (1948).
[2] L.D. Landau, J. Phys. (Moscow) **8**, 201 (1944).
[3] H. Bethe, Phys. Rev. **89**, 1256 (1953).
[4] U. Fano, Annu. Rev. Nucl. Sci. **13**, 1 (1963).
[5] W.T. Scott, Rev. Mod. Phys. **35**, 231 (1963).
[6] N.F. Mott, H. Massey. *The theory of atomic collisions*, 3rd ed., Oxford, Clarendon, 1965.
[7] V.S. Remizovich, D.B. Rogozkin, and M.I. Ryazanov, Sov. J. Part. Nucl. **17**, 1 (1986).
[8] C. Leroy, P.G. Rancoita. *Principles of radiation interaction in matter and detection*, 3rd ed. World Sci., Singapore, 2011.
[9] P. Sigmund. *Particle Penetration and Radiation Effects* Vol. 2. Springer, Heidelberg, 2014.
[10] Particle Data Group, Prog. Theor. Exp. Phys. **2020**, 083C01 (2020).
[11] See, e.g., N.M. Kabachnik, V.N. Kondratev, and O.V. Chumanova, Phys. Stat. Sol. B **145**, 103 (1988); N.M. Kabachnik, NIM B **69**, 76 (1992); G. Schiwietz and P.L. Grande, NIM B **69**, 10 (1992), and refs. therein.
[12] C.N. Yang, Phys. Rev. **84**, 599 (1951).
[13] I. Pomeranchuk, Zh. Exp. Teor. Fiz. **18**, 759 (1948).
[14] L. Meyer, M. Klein, and R. Wedell, Phys. Stat. Sol. B **83**, 451 (1977); K. Ellmer and R. Wedell, Rad. Eff. **59**, 169 (1982).
[15] M.M. Jakas, G.H. Lantschner, J.C. Eckardt, and V.H. Ponce, Phys. Stat. Sol. B **117**, K131 (1983); Phys. Rev. A **29**, 1838 (1984).
[16] S. Shindo, Rad. Eff. **117**, 205 (1991).
[17] V.S. Remizovich, M.I. Ryazanov, and V.V. Frolov, DAN SSSR **282**, 870 (1985) (in Russian).
[18] R. Ishiwari, N. Shiomi, and N. Sakamoto, Phys. Rev. A **25**, 2524 (1982).
[19] N. Sakamoto *et al.* NIM B **69**, 84 (1992).
[20] A. Gras-Marti, NIM B **9**, 1 (1985).
[21] Y. Yamashita, J. Phys. Soc. Jpn. **54**, 2110 (1985).
[22] I.S. Baishev, N.V. Mokhov, and S.I. Striganov, Sov. J. Nucl. Phys. **42**, 745 (1985).
[23] E. Zeitler and H. Olsen, Phys. Rev. A **136**, 1546 (1964).
[24] P. Mertens and T. Krist, NIM B **13**, 95 (1986).
[25] U. Fano, Phys. Rev. **93** (1954) 117.
[26] S.P.A. Sauer, J.R. Sabin, and J. Oddershede, Adv. Quant. Chem. **80**, 225 (2019).
[27] A. Tollestrup and J. Monroe. *Multiple scattering calculations for hydrogen, helium, lithium and beryllium*. NFMCC technical note MC-176 (2000).
[28] J. Wang, R.O. Esquivel, V.H. Smith, and C.F. Bunge, Phys. Rev. A **51**, 3812 (1995).
[29] W. Börsch-Supan, J. Res. Nat. Bur. Stand. B **65**, 245 (1961).
[30] E.J. Williams, Phys. Rev. **58**, 292 (1940).
[31] M.V. Bondarenco, Phys. Rev. D **93**, 036008 (2016).
[32] K.H. Weber and F. Bell, NIM B **159**, 517 (1978).
[33] P. Sigmund and K.B. Winterbon, NIM B **12**, 1 (1985).
[34] Y. Wang *et al.*, Chem. Soc. Rev. **48**, 1492 (2019).
[35] M. Abramowitz, I. A. Stegun. *Handbook of Mathematical Functions*. Washington, DC: Nat. Bur. Stand., 1964.